

# Molecular principles of Piwi-mediated cotranscriptional silencing through the dimeric SFiNX complex

Jakob Schnabl,<sup>1,2,6</sup> Juncheng Wang,<sup>3,6</sup> Ulrich Hohmann,<sup>1,4</sup> Maja Gehre,<sup>1</sup> Julia Batki,<sup>1,5</sup> Veselin I. Andreev,<sup>1,2</sup> Kim Purkhauser,<sup>1</sup> Nina Fasching,<sup>1</sup> Peter Duchek,<sup>1</sup> Maria Novatchkova,<sup>1</sup> Karl Mechtler,<sup>4</sup> Clemens Plaschka,<sup>4</sup> Dinshaw J. Patel,<sup>3</sup> and Julius Brennecke<sup>1</sup>

<sup>1</sup>Institute of Molecular Biotechnology of the Austrian Academy of Sciences (IMBA), Vienna BioCenter (VBC), 1030 Vienna, Austria; <sup>2</sup>Vienna BioCenter PhD Program, Doctoral School at the University of Vienna and Medical University of Vienna, 1030 Vienna, Austria; <sup>3</sup>Structural Biology Program, Memorial Sloan Kettering Cancer Center, New York, New York 10065, USA; <sup>4</sup>Research Institute of Molecular Pathology (IMP), Vienna BioCenter (VBC), 1030 Vienna, Austria

**Nuclear Argonaute proteins, guided by their bound small RNAs to nascent target transcripts, mediate cotranscriptional silencing of transposons and repetitive genomic loci through heterochromatin formation. The molecular mechanisms involved in this process are incompletely understood. Here, we show that the SFiNX complex, a silencing mediator downstream from nuclear Piwi-piRNA complexes in *Drosophila*, facilitates cotranscriptional silencing as a homodimer. The dynein light chain protein Cut up/LC8 mediates SFiNX dimerization, and its function can be bypassed by a heterologous dimerization domain, arguing for a constitutive SFiNX dimer. Dimeric, but not monomeric SFiNX, is capable of forming molecular condensates in a nucleic acid-stimulated manner. Mutations that prevent SFiNX dimerization result in loss of condensate formation in vitro and the inability of Piwi to initiate heterochromatin formation and silence transposons in vivo. We propose that multivalent SFiNX-nucleic acid interactions are critical for heterochromatin establishment at piRNA target loci in a cotranscriptional manner.**

[*Keywords:* *Drosophila* oogenesis; LC8; Panoramix; Piwi; cotranscriptional silencing; heterochromatin formation; molecular condensates; piRNA pathway; transposon silencing]

Supplemental material is available for this article.

Received December 8, 2020; revised version accepted January 22, 2021.

Heterochromatin is critical for maintaining genome integrity in eukaryotes through suppressing transcription of repetitive sequences and preventing them from undergoing ectopic recombination (Slotkin and Martienssen 2007; Fedoroff 2012; Janssen et al. 2018). Initiation and maintenance of heterochromatin require post-translational modifications of histone tails, in particular the deposition of repressive di- and trimethyl groups on lysine 9 of histone H3 (H3K9me2/3) (Allshire and Madhani 2018). As a consequence, various proteins with an affinity for H3K9me2/3 are recruited and stabilized on chromatin. Their biophysical and/or enzymatic activities lead to additional histone modifications, reduced nucleosome dynamics, and increased chromatin compaction (Allshire and Madhani 2018).

Heterochromatin plays a central role in the transcriptional silencing of transposons, selfish genetic elements that make up large parts of plant, fungal, and animal genomes (Slotkin and Martienssen 2007; Fedoroff 2012; Janssen et al. 2018). As transposon insertions resemble endogenous gene loci, mechanisms must exist that direct the heterochromatin machinery specifically to these sites. Eukaryotes employ two principal strategies to form heterochromatin in a sequence-specific manner. The first is based on DNA-binding repressor proteins, which recognize specific motifs in transposon sequences (Yang et al. 2017), and is independent of target locus transcription. The second strategy depends on target locus transcription and is referred to as cotranscriptional gene silencing. It involves small RNAs binding to nuclear Argonaute proteins (Ghildiyal and Zamore 2009) and guiding them to

<sup>5</sup>Present address: Department of Genome Regulation, Max Planck Institute for Molecular Genetics (MPIMG), 14195 Berlin, Germany.

<sup>6</sup>These authors contributed equally to this work.

Corresponding author: julius.brennecke@imba.oeaw.ac.at

Article published online ahead of print. Article and publication date are online at <http://www.genesdev.org/cgi/doi/10.1101/gad.347989.120>.

© 2021 Schnabl et al. This article is distributed exclusively by Cold Spring Harbor Laboratory Press for the first six months after the full-issue publication date (see <http://genesdev.cshlp.org/site/misc/terms.xhtml>). After six months, it is available under a Creative Commons License [Attribution-NonCommercial 4.0 International], as described at <http://creativecommons.org/licenses/by-nc/4.0/>.

complementary, nascent transposon transcripts in chromatin (Grewal 2010; Holoch and Moazed 2015; Martienssen and Moazed 2015; Shimada et al. 2016).

In most animals, cotranscriptional silencing of transposable elements is associated with PIWI-clade Argonaute proteins, which are complexed with PIWI-interacting RNAs (piRNAs) (Siomi et al. 2011; Czech et al. 2018; Ozata et al. 2018). In the *Drosophila melanogaster* ovary, piRNAs encoded by genomic loci that act as heritable libraries of transposon sequences are loaded into three PIWI proteins (Aravin et al. 2007; Senti and Brennecke 2010). One of them, Piwi, acts in the nucleus (Cox et al. 2000; Saito et al. 2006; Brennecke et al. 2007). Piwi-piRNA complexes are recruited to complementary, nascent transcripts and orchestrate heterochromatin formation at hundreds of transposon insertions genome-wide (Wang and Elgin 2011; Sienski et al. 2012; Le Thomas et al. 2013; Rozhkov et al. 2013).

Piwi-mediated silencing requires several general heterochromatin factors such as H3K9 methyl-transferases, histone deacetylases, chromatin remodelers, the SUMOylation machinery, and HP1 proteins that bind the H3K9me2/3 mark and mediate target locus compaction (Sienski et al. 2015; Yu et al. 2015; Iwasaki et al. 2016; Mugat et al. 2020; Ninova et al. 2020). According to current models, only target-engaged Piwi-piRNA complexes are capable of recruiting heterochromatin effectors via dedicated bridging factors (Sienski et al. 2015; Yu et al. 2015). A central bridging factor in this context is the SFiNX complex (a.k.a. Pandas, PICTS, or PNNP complex) (Batki et al. 2019; Fabry et al. 2019; Murano et al. 2019; Zhao et al. 2019). SFiNX is required for piRNA-guided cotranscriptional silencing, and its experimental tethering to nascent RNA induces heterochromatin formation independent of Piwi and piRNAs (Sienski et al. 2015; Yu et al. 2015). The SFiNX complex consists of the orphan protein Panoramic (Panx) and the heterodimeric nuclear RNA export variant Nxf2-Nxt1 (Sienski et al. 2015; Yu et al. 2015; Batki et al. 2019; Fabry et al. 2019; Murano et al. 2019; Zhao et al. 2019). SFiNX has two separable activities. The first involves signaling to the silencing effectors. It resides within the N-terminal, low-complexity region of Panx (Fabry et al. 2019). Experimental recruitment of this ~200-amino-acid polypeptide to a DNA locus is sufficient to induce silencing. However, the same polypeptide is completely inert when recruited to chromatin via a nascent target RNA, arguing for important differences in heterochromatin formation downstream from DNA-binding versus RNA-binding factors. For the cotranscriptional and RNA-directed silencing, SFiNX requires a second activity, which resides in the structured, C-terminal half of Panx that interacts with the Nxf2-Nxt1 heterodimer (Batki et al. 2019). Its molecular function and mechanism are unknown.

Here, we show that SFiNX's ability to mediate heterochromatin formation in a cotranscriptional manner requires SFiNX homodimerization via Cut up (Ctp), the *Drosophila* ortholog of the highly conserved dynein light chain 8. Dimeric SFiNX forms molecular condensates in vitro in a process that is enhanced by nucleic acid binding.

Mutations that impair condensate formation abrogate SFiNX's cotranscriptional silencing capacity in vivo. We propose that multivalent interactions between SFiNX, the nascent RNA, and the underlying chromatin locus enable piRNA-guided cotranscriptional silencing, possibly by retaining the nascent target RNA and bound silencing effectors at chromatin.

## Results

### *The dynein light chain protein Cut up/LC8 is a SFiNX complex subunit*

With the aim to study SFiNX biochemically, we determined all of its core subunits. We immunopurified SFiNX from nuclear lysate of cultured ovarian somatic cells (OSCs) (Niki et al. 2006; Saito et al. 2009) expressing the SFiNX subunit Panx from its endogenous locus and fused to a FLAG-GFP tag (Fig. 1A; Supplemental Table S1). Silver staining of the immunoprecipitate revealed four prominent specific protein bands. Three corresponded to the SFiNX subunits Panx, Nxf2, and Nxt1. The fourth corresponded to Cut up (Ctp), the *Drosophila* ortholog of dynein light chain 8 (LC8) (Dick et al. 1996; Phillis et al. 1996).

Ctp/LC8 was first described as a component of the cytoplasmic dynein multiprotein complex, a minus-end directed microtubule motor (Lo et al. 2001; Makokha et al. 2002). However, SFiNX is a nuclear complex. To confirm the Ctp-SFiNX interaction, we carried out reciprocal coimmunoprecipitation experiments using lysate from OSCs expressing endogenously FLAG-GFP-tagged Ctp (Supplemental Fig. S1A). The SFiNX subunits Panx and Nxf2 robustly and specifically copurified with tagged Ctp (Fig. 1B). To determine the cellular distribution of Ctp in vivo, we analyzed flies expressing GFP-Ctp from a genomic transgene. In ovaries, GFP-Ctp was enriched in foci at the basal surface of the follicular epithelium (potentially muscle attachment sites) and in cytoplasmic foci in nurse cells and the oocyte (Fig. 1C). A substantial fraction of GFP-Ctp, however, localized to the nucleus, which was also seen in tissues such as the wing imaginal disc or larval fat body (Supplemental Fig. S1B). These findings were consistent with a Ctp-SFiNX interaction and pointed to a general role of Ctp in nuclear processes (Jespersen et al. 2019).

To investigate whether Ctp acts in the piRNA pathway, we used a cotranscriptional silencing assay in OSCs where the silencing capacity of a protein of interest can be determined by recruiting it via the  $\lambda$ N-boxB system to nascent transcripts expressed from a stably integrated GFP-reporter transgene (Fig. 1D; Sienski et al. 2015; Yu et al. 2015). Tethering of the SFiNX subunits Panx or Nxf2 results in ~20-fold reporter silencing via heterochromatin formation (Batki et al. 2019). Recruitment of Ctp led to a similarly strong repression (Fig. 1E). Reporter silencing by Ctp was dependent on SFiNX, as depletion of Panx abrogated the silencing response elicited by  $\lambda$ N-Ctp recruitment, as also seen for tethering of  $\lambda$ N-Nxf2 (Fig. 1F;

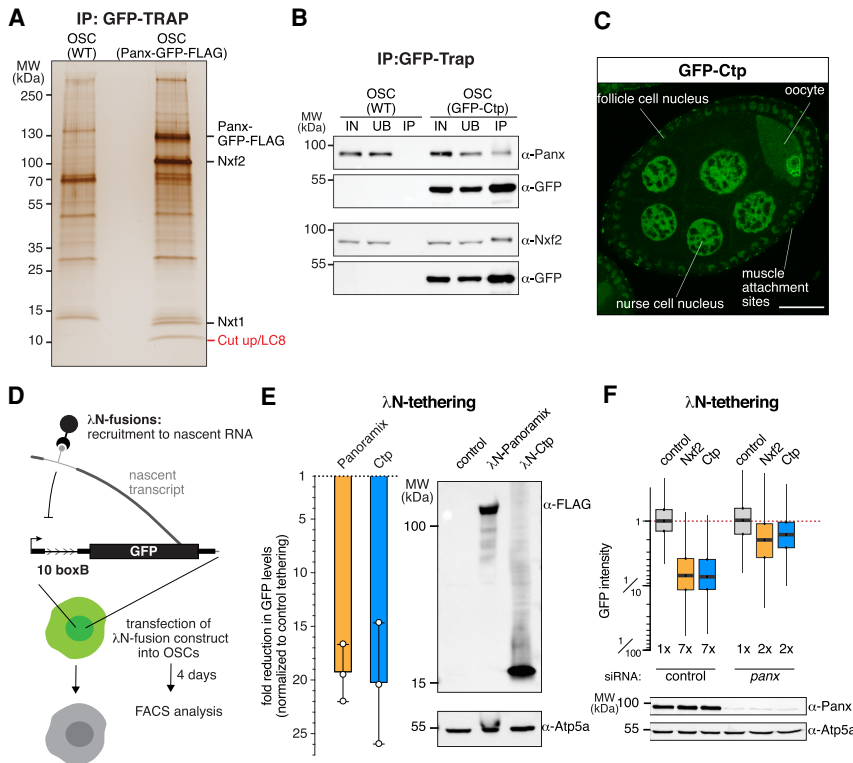


**Figure 1.** The dynein light chain Cut up/LC8 is an integral SFiNX complex subunit. (A) Silver-stained SDS-PAGE ([left] molecular weight marker) of immunoprecipitated Panx (from endogenously FLAG-GFP-tagged OSC line) and control (from wild-type OSCs). Indicated bands were identified using mass spectrometry. (B) Western blot analysis indicating coimmunoprecipitation of endogenously tagged Ctp from OSCs with Panx and Nxf2 (control: wild-type OSCs). (C) Confocal image of *Drosophila* egg chamber showing GFP-tagged Ctp. Scale bar, 20 $\mu$ m. (D) Cartoon showing the cotranscriptional silencing reporter system in OSCs. (E, left) Bar diagram indicates fold repression of the GFP reporter after transfection of indicated  $\lambda$ N-tagged proteins normalized to control (data represent mean  $\pm$  SD of three biological replicates). (Right) Western blot analysis showing expression of indicated  $\lambda$ N fusion proteins in OSCs (Atp5a: loading control). (F, top) Box plots showing GFP reporter levels in OSCs 5 d after transfection with siRNAs against control or *panx* and 3 d after transfection with plasmids expressing indicated  $\lambda$ N fusion proteins (numbers indicate fold repression values normalized to control; box plots indicate median, first, and third quartiles [box]; whiskers show 1.5 $\times$  interquartile

range; outliers were omitted;  $n = 2500$  cells). The western blot shows Panx protein levels in control versus *panx* siRNA transfected OSCs (Atp5a: loading control).

Supplemental Fig. S1C). Thus, Ctp is a fourth core subunit of the SFiNX complex.

### Ctp is required for SFiNX function

*panx* mutant flies are viable but sterile, exhibiting strong transposon derepression. In contrast, mutations in the ubiquitously expressed *ctp* gene are lethal (Dick et al. 1996; Phillis et al. 1996). To ask whether Ctp is required for piRNA pathway function, we depleted Ctp in OSCs using RNAi and observed derepression of *gypsy* and *mdg1*, two LTR retroelements under piRNA pathway control in OSCs (Fig. 2A,B). Ctp depletion also resulted in reduced Panx and Nxf2 protein levels (but not mRNA levels) (Fig. 2B; Supplemental Fig. S2A). Considering the reciprocal stabilization of Panx and Nxf2 (Batki et al. 2019; Fabry et al. 2019; Murano et al. 2019; Zhao et al. 2019), our data suggest that Ctp is required for the function and the assembly of the SFiNX complex.

Ctp is implicated in diverse dynein-dependent and -independent cellular processes (Barbar 2008; Rapali et al. 2011b), arguing that the transposon silencing defects in Ctp-depleted cells could be indirect. To determine whether Ctp is directly required for SFiNX function, we first defined the physical interaction between Ctp and the other SFiNX subunits. Ctp/LC8 proteins are homodimers that interact with many cellular proteins. Two symmetric binding grooves at the dimer interface bind peptides, which harbor a consensus motif with a "TQT"

anchor (Fig. 2C; Barbar 2008; Rapali et al. 2011b). To determine which SFiNX subunit interacts directly with Ctp, we predicted potential Ctp/LC8 binding sites using computational tools (Erdős et al. 2017; Jespersen et al. 2019). The only two predicted motifs were within a short, disordered stretch of the Panx C terminus (NAATQTE and DAGTQVR). Both of these sites are evolutionarily conserved (Fig. 2C). To test whether Panx interacts with Ctp via the predicted motifs, we performed co-IP experiments using lysates from *Drosophila* Schneider 2 cells (S2) transiently expressing GFP-Ctp and FLAG-Panx. Only the C-terminal portion of Panx (amino acids 447–541), including the two predicted binding sites, interacted with Ctp (Fig. 2D). As this region does not harbor the binding site for the Nxf2–Nxt1 heterodimer, these results establish Panx as the Ctp interaction partner in SFiNX. In order to disrupt the Ctp–Panx interaction, we introduced alanine substitutions into the TQT/V core motifs in Panx. Mutation of both sites, but not of either site alone, abrogated the interaction (Fig. 2E; Supplemental Fig. S2B). Thus, Panx harbors two functional Ctp/LC8 binding sites.

To determine whether Ctp is directly required for Panx and, therefore, SFiNX function, we generated flies harboring alanine substitutions in the TQT/V core of both Ctp interaction sites in the endogenous *panx* locus (*panx* [Ctp-*mut*]) (Supplemental Fig. S2C). Homozygous *panx* [Ctp-*mut*] flies were viable and exhibited reduced Panx protein levels (Fig. 2F), consistent with the reduced Panx levels in OSCs lacking Ctp (Fig. 2B). *panx*[Ctp-

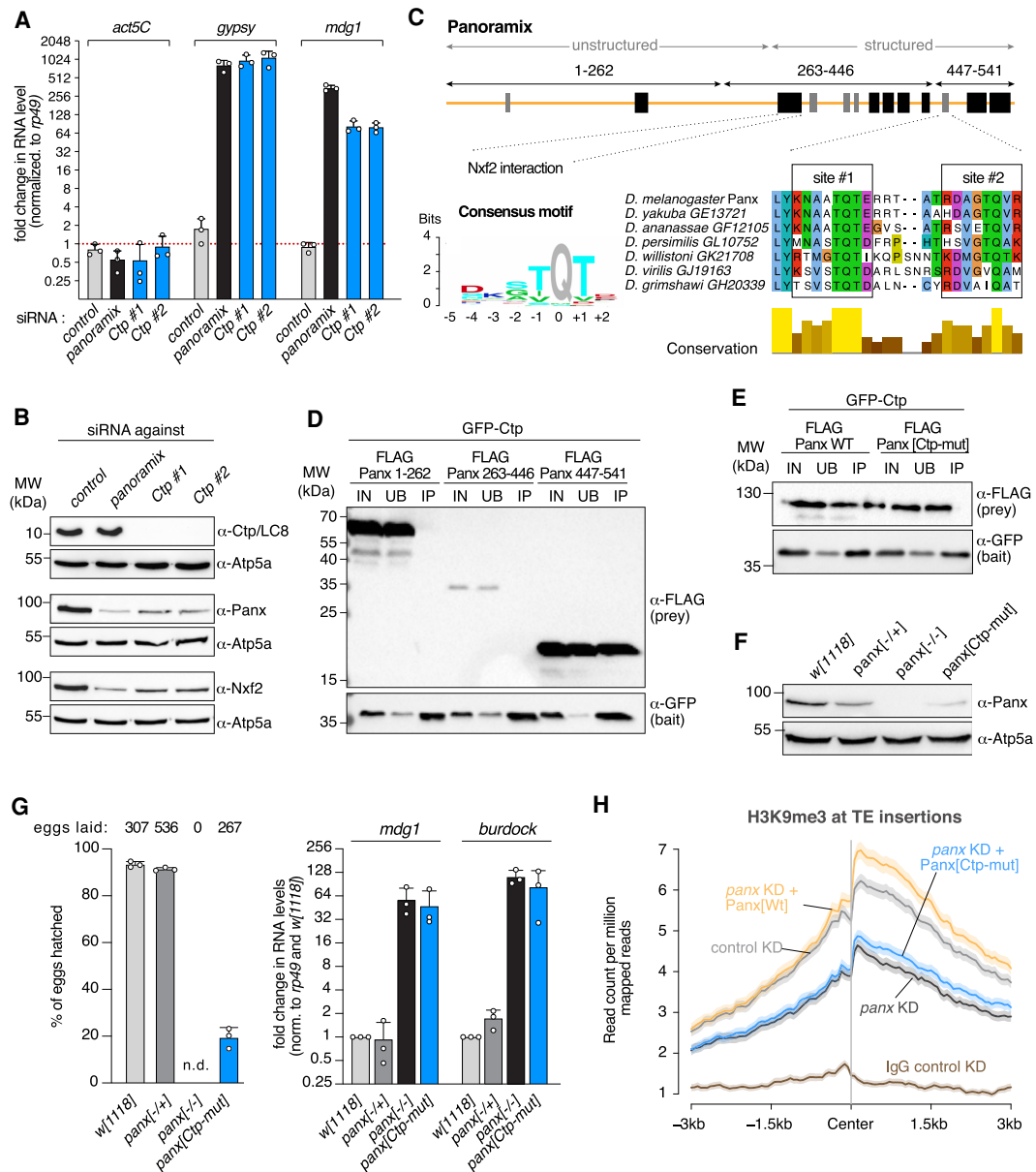


**Figure 2.** Ctp is required for SFiNX-mediated transposon silencing. (A) Bar graph showing mRNA levels (normalized to *rp49* levels) of the endogenous LTR retrotransposons *gypsy* and *mdg1* after depletion of Panx or Ctp (two independent siRNAs). *actin5C* mRNA levels served as control. Data represent mean  $\pm$  SD of three independent experiments. (B) Western blot showing levels of indicated proteins after depletion of Panx or Ctp (Atp5a: loading control). (C) Schematic representation of Panx, indicating secondary structure elements ([black]  $\alpha$  helices, [gray]  $\beta$  strands), and the two Ctp binding sites and their evolutionary conservation are shown below. The sequence logo depicts the consensus Ctp/LC8 binding motif (Rapali et al. 2011a). Protein regions tested in D are indicated. (D,E) Western blot analyses of GFP-Ctp immunoprecipitation experiments using lysate from S2 cells transfected with indicated FLAG-Panx expression plasmids (relative amount loaded in immunoprecipitation lanes: 4 $\times$ ). (IN) Input, (UB) unbound, (IP) immunoprecipitate. (F) Western blot showing Panx levels in ovarian lysates from flies of indicated genotype (Atp5a: loading control). (G) The left bar graph shows hatching rates of eggs laid by flies of indicated genotype (data represent mean  $\pm$  SD of three independent replicates). The right graph shows mRNA levels of somatic (*mdg1*) and germline (*burdock*) transposons in total ovarian RNA from flies of indicated genotype (normalized to *rp49* and control flies; data represent mean  $\pm$  SD of three independent replicates). (H) Meta profiles showing H3K9me3 levels (determined by CUT&RUN) in a 6-kb window around 381 piRNA-controlled transposon insertions ("center") in OSCs transfected with indicated siRNAs (control or *panx* KD) and rescue constructs (IgG served as control). Shading indicates standard error of mean (SEM) of two replicates.

*mut*] flies showed reduced fertility (egg hatching rate:  $\sim$  20%) and displayed transposon derepression in the ovarian soma and germline to an extent resembling that of

*panx*-null mutants (Fig. 2G). In comparison, heterozygous *panx*[+/-] flies, which have Panx protein levels comparable with the *panx*[Ctp-*mut*] mutant, exhibited no

transposon silencing or fertility defects (Fig. 2F,G). Consistent with the strong transposon silencing defects, OSCs expressing Panx[*Ctp-mut*] instead of wild-type Panx displayed reduced H3K9me3 levels around piRNA-controlled transposon insertions (Fig. 2H; Sienski et al. 2012, 2015). Taken together, our data establish that Ctp is directly required for SFiNX function.

#### *Ctp does not connect SFiNX to other protein complexes*

Ctp/LC8 has originally been proposed to function as cargo adaptor for the dynein motor complex (Fan et al. 2001; Pfister et al. 2006). We hypothesized that Ctp might analogously connect SFiNX to downstream silencing effec-

tors. To identify Ctp interaction partners, we performed Ctp coimmunoprecipitation experiments from OSCs and from fly ovaries expressing FLAG-GFP-Ctp (Fig. 1C; Supplemental Fig. S1A). Quantitative, label-free mass spectrometry revealed a large number of proteins copurifying with Ctp (Fig. 3A,B). We identified 19 out of 30 Flybase-annotated Ctp interactors (Thurmond et al. 2019), including proteins of the dynein motor complex (Sw, Dlc90F, and Robl), the microtubule linked protein Kank, and the centriolar protein Ana2 (Supplemental Table S2). In addition to known cytoplasmic interactors, several nuclear proteins were enriched in Ctp immunoprecipitates. Besides the SFiNX subunits Panx, Nxf2, and Nxt1, these included a complex involved in telomere biology

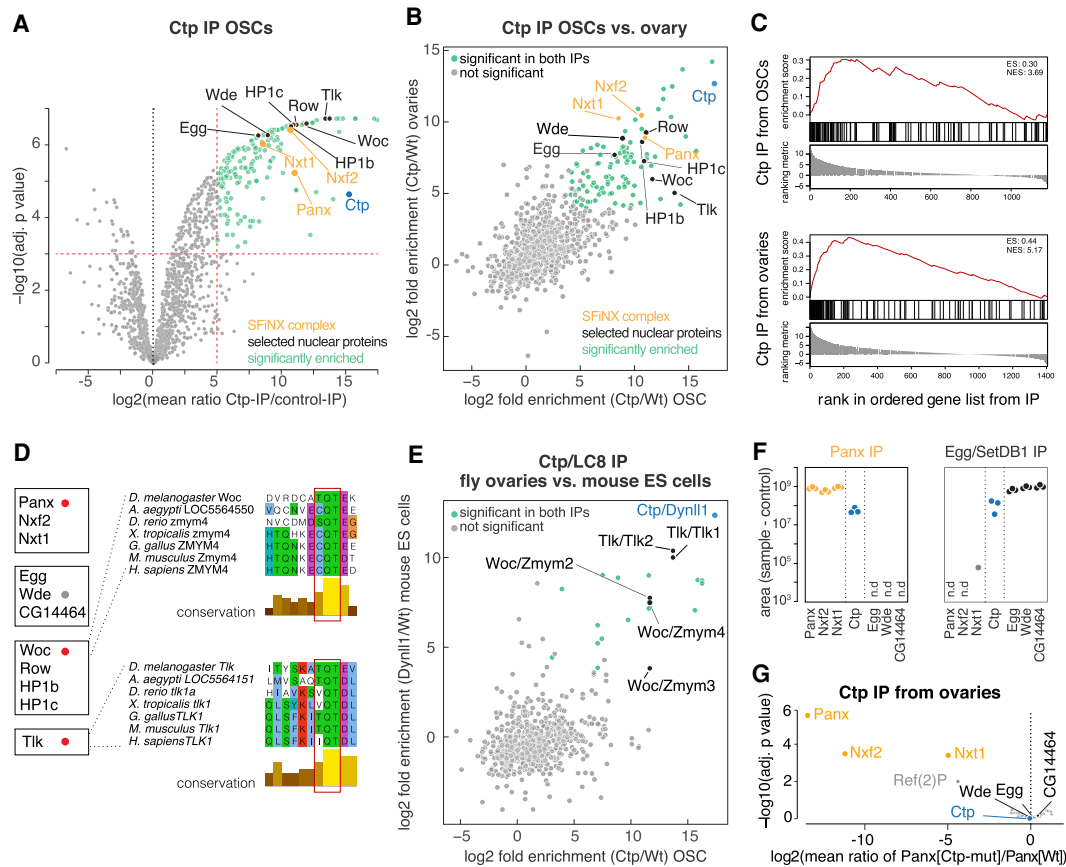


**Figure 3.** Ctp mediates dimerization of diverse nuclear protein complexes. (A) Volcano plot showing fold enrichments versus statistical significance (determined by quantitative mass spectrometry) of proteins in FLAG-GFP-Ctp coimmunoprecipitates versus control ( $n = 3$  biological replicates; experimental OSCs express endogenously tagged Ctp; control: wild-type OSCs). The bait (Ctp) and selected interacting nuclear proteins are labeled; red lines indicate applied significance cutoffs. (B) Scatter plot showing fold enrichments (versus control) of proteins coimmunoprecipitating with Ctp from OSC versus ovary lysates. The bait (Ctp) and selected interacting nuclear proteins are labeled. (C) Enrichment of predicted Ctp/LC8 motifs in Ctp copurifying proteins (from OSCs [top] and from ovaries [bottom]) determined by gene set enrichment analysis. Protein lists were ranked by their fold enrichment (ranking metric) in the respective coimmunoprecipitation experiments. Ctp hub (Jespersen et al. 2019) was used for Ctp motif prediction. (D) Selected nuclear Ctp interactors grouped into known protein complexes. (Dots) Predicted Ctp binding motifs, (red) experimentally confirmed, (gray) not confirmed. (Right) Protein sequence alignments of indicated Ctp binding sites are shown; TQT motifs (mutated in Supplemental Fig. S3A,B) are highlighted. (E) Scatter plot showing fold enrichments (vs. control) of proteins coimmunoprecipitating with Ctp (from OSCs) or with LC8/Dynll1 from mouse ES cells. The bait (LC8) and selected interacting nuclear proteins are labeled. (F) Absolute peak intensities of peptides from indicated proteins in Panx or Egg coimmunoprecipitates (values of matched controls were subtracted from experimental values;  $n = 3$  replicates). (n.d.) Not detected. (G) Volcano plot showing fold enrichment of proteins (determined by quantitative mass spectrometry) in FLAG-GFP-Ctp coimmunoprecipitates from *panx*[*Ctp-mut*] versus wild-type ovaries. ( $n = 3$  biological replicates).

and transcriptional regulation (Woc, Row, HP1b, and HP1c) (Font-Burgada et al. 2008; Kessler et al. 2015), the Tousled-like kinase (regulator of replication-dependent chromatin assembly) (Silljé and Nigg 2001), and the H3K9 methyltransferase complex consisting of Eggless/SetDB1 and its partner proteins Windei/ATF7IP and CG14464/ARLE-14 (Koch et al. 2009; Mutlu et al. 2018; Osumi et al. 2019).

To understand how Ctp binds such a diverse set of proteins, we explored whether the identified interactors contained "TQT" binding motifs. Ctp copurifying factors were enriched in predicted high-scoring Ctp binding motifs (Fig. 3C). For most of the protein complexes analyzed, only one subunit harbored a predicted Ctp binding motif. For SFiNX, this was Panx. For the Woc-Row-HP1b-HP1c complex, this was Woc, the fly ortholog of the mammalian Zmym2/3/4 transcriptional regulators, and mutation of the TQT motif disrupted the physical interaction with Ctp (Supplemental Fig. S3A). Similar results were obtained for Tousled-like kinase (Supplemental Fig. S3B). Our data are consistent with the proposal that Ctp/LC8 homodimers act as a dimerization hub for various client proteins possessing an accessible TQT binding site (Barbar 2008; Rapali et al. 2011b).

Ctp is highly conserved, with the fly and human proteins (LC8/Dynll1) being 96% identical over their entire length. To investigate whether LC8's interaction with nuclear factors is also conserved, we performed co-IP experiments in mouse ES (mES) cells. Mouse LC8 is present in both cytoplasm and nucleus, and LC8 coimmunoprecipitates with Zmym2/4 (the mouse ortholog of Woc) and the Tousled-like kinases (Fig. 3D,E; Supplemental Fig. S3C, D). The LC8 binding sites in Woc/Zmym2/4 and Tousled-like kinase are evolutionarily conserved from flies to mammals, indicating that the function of Ctp/LC8 in the nucleus is ancient and not connected solely to SFiNX, a protein complex specific to Diptera.

Ctp's ability to bind diverse nuclear protein complexes might allow it to connect SFiNX to downstream heterochromatin effectors. Notably, the Eggless/SetDB1 complex, a H3K9 methyltransferase involved in heterochromatin establishment, was highly enriched in the Ctp coimmunoprecipitates (Fig. 3A,B). SetDB1 and its cofactor Windei/Atf7IP act downstream from SFiNX during piRNA-guided heterochromatin formation in OSCs and fly ovaries (Sienski et al. 2015; Yu et al. 2015; Osumi et al. 2019). To assay for a physical interaction between SFiNX and the SetDB1 complex (potentially mediated by Ctp), we used quantitative mass spectrometry to identify proteins copurifying with SFiNX (endogenously tagged Panx) or the SetDB1 complex (endogenously tagged Eggless) (Supplemental Fig. S3E). Ctp was among the highest coenriched proteins in both experiments. However, SFiNX subunits were not present in the SetDB1 complex purification and vice versa (Fig. 3F; Supplemental Fig. S3F, G), arguing against a direct SFiNX-SetDB1 complex interaction and suggesting that Ctp interacts with both complexes independently.

To further test this prediction, we performed Ctp coimmunoprecipitation experiments from ovary lysates of

wild-type flies versus flies expressing *panx*[*Ctp-mut*]. Among the 115 proteins that were highly enriched (>30-fold) in Ctp immunoprecipitates (Fig. 3B), only the SFiNX subunits Panx, Nxf2, and Nxt1 failed to interact with Ctp in *panx*[*Ctp-mut*] lysates, while Ctp binding to the SetDB1 complex was unchanged (Fig. 3G). Altogether, our findings do not support a model where Ctp connects SFiNX to heterochromatin effectors. Instead, they suggest that Ctp is part of several, physically separate cytoplasmic and nuclear protein complexes. Considering that the Ctp/LC8 homodimer harbors two symmetric binding sites for TQT motif-containing peptides, our data support a role for Ctp as a versatile dimerization module for diverse cellular protein complexes (Barbar 2008; Rapali et al. 2011b; Jespersen et al. 2019).

#### *The SFiNX complex is a homodimer*

To test whether SFiNX forms Ctp-mediated dimers or oligomers, we used the OSC line harboring a heterozygous, tagged *panx* allele and performed coimmunoprecipitation followed by western blot. This revealed that tagged and untagged Panx copurify (Fig. 4A). Similarly, transiently expressed GFP-Panx and FLAG-Panx interact, and this interaction was dependent on the two Ctp binding sites in Panx, indicating that Ctp is required for SFiNX oligomerization (Supplemental Fig. S4A).

To more precisely characterize the oligomerization mode of Panx, we purified Ctp together with Panx peptides harboring either TQT/V site #1, site #2, or both. Size exclusion chromatography coupled to multiangle light scattering (SEC-MALS) revealed that the molecular weight of the protein complexes corresponded to either one Ctp homodimer with two single-TQT/V Panx peptides (predicted MW: 23.5 and 23.8 kDa) or two Ctp homodimers with two dual-TQT/V Panx peptides (predicted MW: 47.5 kDa) (Fig. 4B). Isothermal titration calorimetry (ITC) measurements revealed comparable affinities for the two individual TQT/V sites in Panx (TQT peptide: Kd ~75 nM; TQV peptide: Kd ~140 nM), in line with previous measurements for unrelated Ctp/LC8-peptide complexes (Kidane et al. 2013). A Panx peptide with both core TQT/V motifs mutated to alanine showed no binding to Ctp (Supplemental Fig. S4B). Thus, Ctp mediates homodimerization of Panx (and SFiNX) via two TQT/V motifs and does not promote the formation of higher order oligomers, even though theoretically possible given the two Ctp binding sites in Panx.

Using the recombinant Ctp-Panx (single TQT/V site) complexes, we determined their atomic structures at 1.42 Å resolution for site #1 and 1.79 Å resolution for site #2, respectively (Fig. 4C; Supplemental Fig. S4C; Supplemental Table S3). TQT/V peptides #1 and #2 adopt an almost identical binding mode to Ctp that is similar to known Ctp/LC8-peptide complexes (Liang et al. 1999; Gallego et al. 2013): The Ctp dimer contains two hydrophobic-lined grooves on opposite faces, allowing two parallel Panx peptides to bind (Fig. 4D). The TQT/V motif is recognized through a hydrogen-bonding network involving residues from both Ctp monomers (Fig. 4E). To

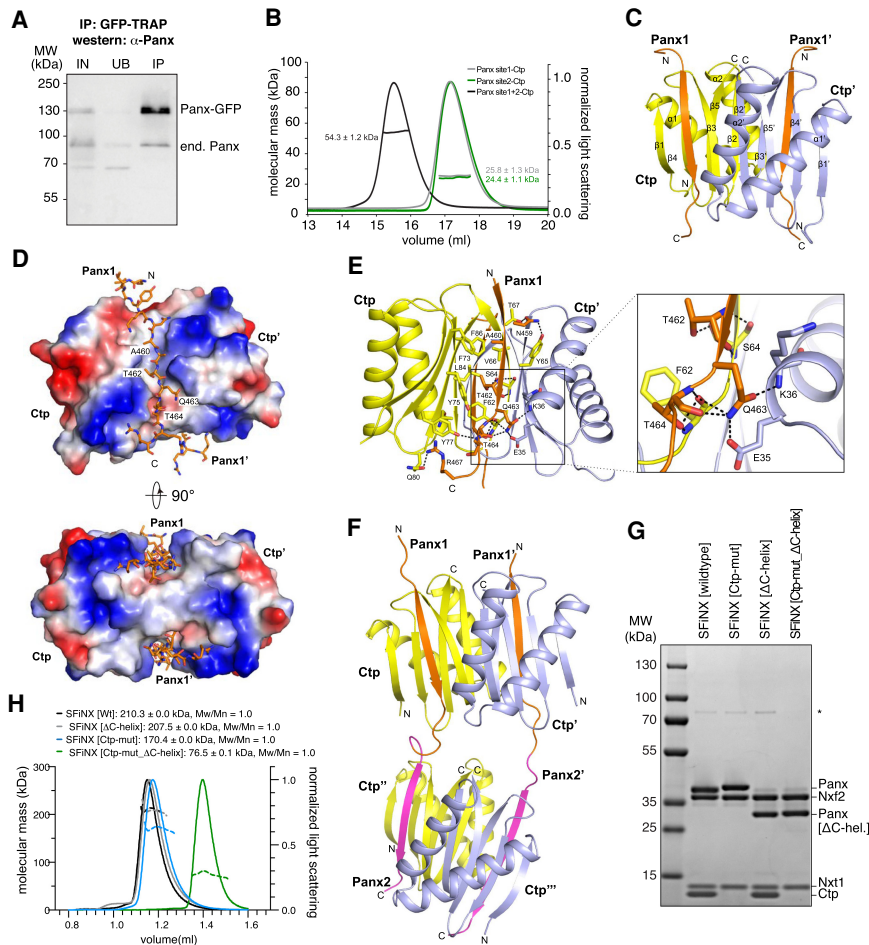


**Figure 4.** The SFiNX complex is a homodimer. (A) Western blot analysis of a Panx-GFP immunoprecipitation experiment from OSCs harboring one GFP-tagged and one wild-type *panx* allele. (IN) Input, (UB) unbound, (IP) immunoprecipitate. (B) Molecular weight determination of Ctp in complex with Panx peptides containing Ctp binding site #1 (TQT site), site #2 (TQV site), or both sites as measured by SEC-MALS. (C) Ribbon representation of the structure of a Ctp homodimer (monomers in yellow and cyan) in complex with two Panx peptides containing the Ctp interacting site #1 (TQT site). (D) Electrostatic surface representations of the Ctp homodimer in complex with two Panx peptides containing the Ctp interacting site #1 (TQT site; shown in stick representation). (E) Inter-molecular interactions (hydrophobic and hydrogen bonding networks) between the Ctp dimer (monomers in yellow and cyan) and a Panx peptide containing the Ctp interacting site #1 (orange). The TQT motif recognition is shown in the close-up. (F) Ribbon representation of the structure of two Ctp dimers (yellow and blue) in complex with two Panx peptides containing Ctp interacting sites #1 and #2. (G) Coomassie-stained SDS PAGE showing recombinant SFiNX complex variants with indicated protein subunits analyzed in H. (\*) HSP70 as determined by mass spectrometry. (H) SEC-MALS chromatogram and determined molecular weight of indicated SFiNX complex variants (from G).

determine the conformation of Ctp with tandem TQT/V sites, we solved the crystal structure of the Ctp–Panx (dual TQT/V-site) complex at 2.5 Å resolution (Fig. 4F; Supplemental Table S3). This showed that two Ctp homodimers bind the two closely spaced TQT/V motifs from a pair of parallel aligned Panx peptides. The Ctp–Panx interaction for each site is highly similar to the complexes harboring single TQT/V peptides (RMSDs 0.25 for peptide #1 and 0.31 for peptide #2). Our structural analyses confirm that the two tandem TQT/V motifs in Panx are compatible with homodimerization via two Ctp dimers.

To test whether Ctp-mediated Panx dimerization also occurs in the context of the SFiNX complex, we purified recombinant SFiNX consisting of Panx[263–541], Nxf2 [541–841], Nxt1, and Ctp from insect cells. This complex lacks the N-terminal low-complexity region of Panx (implicated in silencing) and the N-terminal double RRM-LRR domains in Nxf2 (implicated in RNA binding) (Batki et al. 2019; Fabry et al. 2019; Murano et al. 2019; Zhao et al. 2019). All four proteins formed a stable, uniform complex with a molecular weight corresponding to a homodimer consisting of two molecules each of Panx, Nxf2, and Nxt1 plus four molecules of Ctp. (Fig. 4G,H, note the double intensity of the Ctp band compared with the Nxt1 band).

We previously reported that the ternary protein complex consisting of Nxf2–Nxt1 and C-terminally truncated Panx is monomeric (Batki et al. 2019), which is to be expected as, in this complex, Panx lacks the C-terminal 95 amino acids, including both TQT/V motifs. We hypothesized that SFiNX should also be monomeric when coexpression of Ctp is omitted, even when the Panx C terminus is intact. As expression of wild-type Panx led to the copurification of endogenous LC8 from insect cells, we expressed the Panx[Ctp-mut] variant for this experiment. The ternary Panx[263–541] Ctp-mut–Nxf2[541–841]–Nxt1 complex, despite lacking Ctp, was still a dimer in solution (Fig. 4G,H). This suggested that the very C terminus of Panx harbors an additional dimerization activity, a model consistent with observations that several Ctp client proteins harbor alternative dimerization entities adjacent to their Ctp binding sites (Wang et al. 2004; Barbar 2008). Immediately downstream from the two TQT/V motifs, Panx harbors two predicted  $\alpha$  helices. Truncation of the two helices alone did not prevent dimer formation of the quaternary SFiNX complex containing Ctp (Fig. 4G,H) but, in combination with mutation of the two TQT/V motifs (Panx[Ctp-mut\_ $\Delta$ C-helix]), resulted in a monomeric complex (Fig. 4G,H). Taken together, SFiNX is a homodimeric complex consisting of two

Panx subunits, two Nxf2–Nxt1 heterodimers, and two Ctp homodimers. The two C-terminal  $\alpha$  helices in Panx probably serve as an initial dimerization unit, ensuring that Ctp binding enforces homodimerization rather than bridging SFiNX to other Ctp client proteins.

#### *SFiNX dimerization is required for cotranscriptional silencing*

To determine whether SFiNX dimerization is required for piRNA-guided cotranscriptional silencing, we probed the ability of Panx variants, lacking either one of its two dimerization activities alone or both together, to restore transposon silencing in OSCs depleted for endogenous Panx. While deletion of the two C-terminal  $\alpha$  helices (Panx [ $\Delta$ C-helix]) impacted SFiNX silencing activity only mildly, mutation of the two Ctp binding motifs (Panx[Ctp-mut]) reduced it markedly. Deletion of both dimerization interfaces (Panx [ $\Delta$ C-term]) resulted in complete loss of SFiNX activity (Fig. 5A), indicating that dimerization is required for SFiNX function.

We hypothesized that if homodimerization is the sole function of the Panx C terminus, replacing it with a heterologous dimerization module should rescue SFiNX functionality. To test this, we replaced either the internal 15-amino acid peptide harboring both Ctp-binding motifs (Panx [ $\Delta$ Ctp-Gcn4]) or the entire Panx C terminus (lacking both Ctp binding sites and the C-terminal helices; Panx [ $\Delta$ C-term-Gcn4]) with a 32-amino-acid motif from the yeast transcription factor Gcn4 that forms a coiled coil sufficient to promote dimerization (Fig. 5B; O’Shea et al. 1991; Goldman et al. 2019). Gcn4 coiled-coil-mediated dimerization was confirmed using transiently expressed tagged Panx variants (Supplemental Fig. S5A). When tested in OSC rescue experiments, both SFiNX variants harboring the Gcn4 coiled coil exhibited substantially improved transposon silencing activity compared with their dimerization-defective counterparts (Fig. 5A; Supplemental Fig. S5B,C).

We probed the functionality of the same Panx variants in flies. *panx* mutant females expressing tagged wild-type Panx or any of the dimerization-defective variants from a genomic transgene were analyzed for sterility and transposon silencing (Supplemental Fig. S5D). The results confirmed that SFiNX[Panx Ctp-mut] is a strong mutant (egg hatching: ~4%) and that monomeric SFiNX[Panx  $\Delta$ C-term] is equivalent to a *panx*-null mutant (the few laid eggs displayed a collapsed morphology, and egg hatching was 0%) (Fig. 5C). Expression of Panx variants harboring the Gcn4 coiled coil substantially restored transposon silencing and fertility compared with their respective dimerization-defective counterparts (Fig. 5D). Thus, a heterologous protein dimerization domain can largely replace the function encoded in the 95-amino-acid Panx C terminus.

To determine whether dimerization of SFiNX is required for interaction with upstream or downstream factors, we used the silencing reporter assay that allows comparing DNA targeted and RNA targeted silencing (Fig. 5E; Batki et al. 2019). We first recruited the different

SFiNX variants to the nascent reporter RNA and tested their silencing capacity. In this assay, events upstream of SFiNX action (e.g., its recruitment to the target by Piwi) are bypassed and only the ability of SFiNX to mediate cotranscriptional silencing is assessed. Deletion of the C-terminal helices did not impair SFiNX functionality. However, mutation of both Ctp binding sites led to substantially reduced activity (Fig. 5F; Supplemental Fig. S5E). The monomeric SFiNX (Panx [ $\Delta$ C-term]) complex lost all cotranscriptional silencing capacity. Gcn4 coiled-coil-mediated dimerization fully restored SFiNX silencing ability, even for the variant lacking 95 C-terminal amino acids in Panx (Fig. 5F; Supplemental Fig. S5E). Thus, dimerization of SFiNX is required downstream from its recruitment to a target RNA via Piwi.

To assay whether SFiNX dimerization is required for recruiting heterochromatin effectors, we targeted monomeric (Panx [ $\Delta$ C-term]) or dimeric, wild-type SFiNX directly to the reporter locus using UAS-sites upstream of the promoter and fusion proteins between Panx and the Gal4 DNA binding domain. Monomeric SFiNX was as potent at transcriptional silencing as dimeric SFiNX (Fig. 5F; Supplemental Fig. S5E). Thus, SFiNX dimerization is not required for it to signal to the downstream silencing machinery. Taken together, we conclude that dimerization of SFiNX is required for the N-terminal silencing domain within Panx to silence the target locus in a cotranscriptional manner, meaning when recruited to chromatin via the nascent target RNA.

#### *Dimeric SFiNX interacts with nucleic acids*

To understand how dimerization enables SFiNX’s cotranscriptional silencing activity, we characterized monomeric versus dimeric SFiNX complexes in vitro. We first assessed whether SFiNX interacts with nucleic acids using electrophoretic mobility shift assays (EMSA). We purified recombinant SFiNX lacking the N-terminal low-complexity domain of Panx (involved in silencing) and lacking both RRM-LRR domains of Nxf2 (implicated in RNA binding) (Fig. 4G; Batki et al. 2019; Fabry et al. 2019; Murano et al. 2019; Zhao et al. 2019). Dimeric SFiNX interacted with nucleic acids, preferentially binding single-stranded (ss) RNA, having lower yet comparable affinities for double-stranded (ds) DNA and dsRNA, and binding ssDNA weakly (Fig. 6A,B; Supplemental Fig. S6A). Deletion of the Panx C-terminal helices or mutating both Ctp binding sites had a substantial impact on nucleic acid binding (measured for ssRNA) (Fig. 6C; Supplemental Fig. S6B). Simultaneous deletion of both dimerization interfaces abolished RNA binding (Fig. 6C; Supplemental Fig. S6B). Thus, SFiNX binds to nucleic acids in a dimer-dependent manner.

The interaction of SFiNX with dsDNA suggested a putative model where SFiNX enables or stimulates cotranscriptional silencing by tethering the nascent target RNA (via an interaction with Piwi) to the underlying chromatin locus. To test this, we set out to identify mutations in SFiNX that allow dimer formation yet prevent DNA binding. Upstream of the Ctp binding sites, Panx harbors

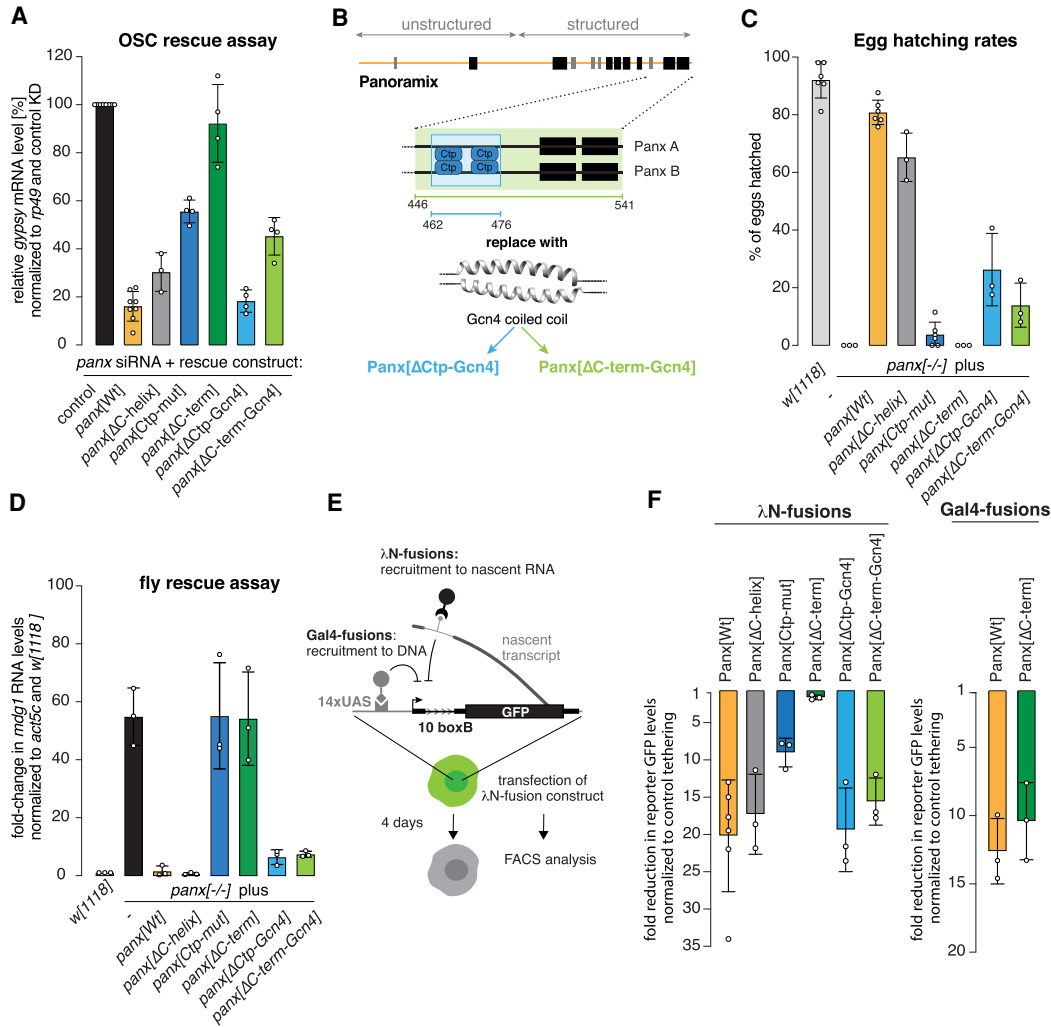


**Figure 5.** Dimerization is required for SFiNX to silence in a cotranscriptional manner. (A) Bar graph showing the transposon repression rescue potential of indicated *Panx* expression constructs transfected into OSCs depleted of endogenous *Panx*. *gypsy* levels were determined via qRT-PCR (at least three biological replicates are shown; error bars: SD). (B) Cartoon representation of the “bypass” strategies using the yeast GCN4 coiled-coil domain. Internal replacement of both Ctp binding sites (blue) or replacement of the entire C-terminal domain of *Panx* (green) are shown. (C) Bar graph showing hatching rates of eggs laid by flies with indicated genotype (at least three biological replicates are shown; error bars: SD). (D) Bar graph showing mRNA levels of the LTR retrotransposon *mdg1* determined via qRT-PCR in ovaries of indicated genotypes. Expression levels were normalized to *w*[1118] controls and *act5C* ( $n = 3$  biological replicates; error bars: SD). (E) Cartoon showing the OSC reporter system that allows analysis of cotranscriptional ( $\lambda$ N-recruitment) and transcriptional (Gal4 recruitment) silencing. (F) Bar diagrams showing silencing potential (GFP repression) of indicated  $\lambda$ N (left) or Gal4 (right) fusion proteins normalized to control (data represent mean + SD of at least three independent experiments).

an  $\alpha$ -helical region rich in positively charged residues and exhibiting remote similarity to a helix-turn-helix motif, a widespread domain that binds dsDNA. Mutation of nine positively charged amino acids in this region (Fig. 6D) of *Panx* resulted in a recombinant SFiNX complex that, in respect to dimer formation, behaved as the wild-type complex but that was incapable of binding to dsDNA and showed weaker binding to ssRNA (Fig. 6E; Supplemental Fig. S6C). Genetic rescue experiments indicated that this DNA-binding-defective *Panx* mutant is strongly impaired in compensating for endogenous *Panx* in OSCs (Fig. 6F; Supplemental Fig. S6D). When recruited to the nascent reporter RNA via the  $\lambda$ N-boxB system, DNA-binding-defi-

cient *Panx* was only moderately impaired in its ability to support cotranscriptional silencing (Fig. 6F; Supplemental Fig. S6E). Our findings indicate that SFiNX’s ability to bind DNA is an important, but not the only, feature that is required for its cotranscriptional silencing capacity.

#### *SFiNX* can form molecular condensates in a nucleic acid-stimulated manner

Multivalent protein–protein and protein–nucleic acid interactions have been implicated in many chromatin-related processes (e.g., Narlikar 2020). Intrigued by the

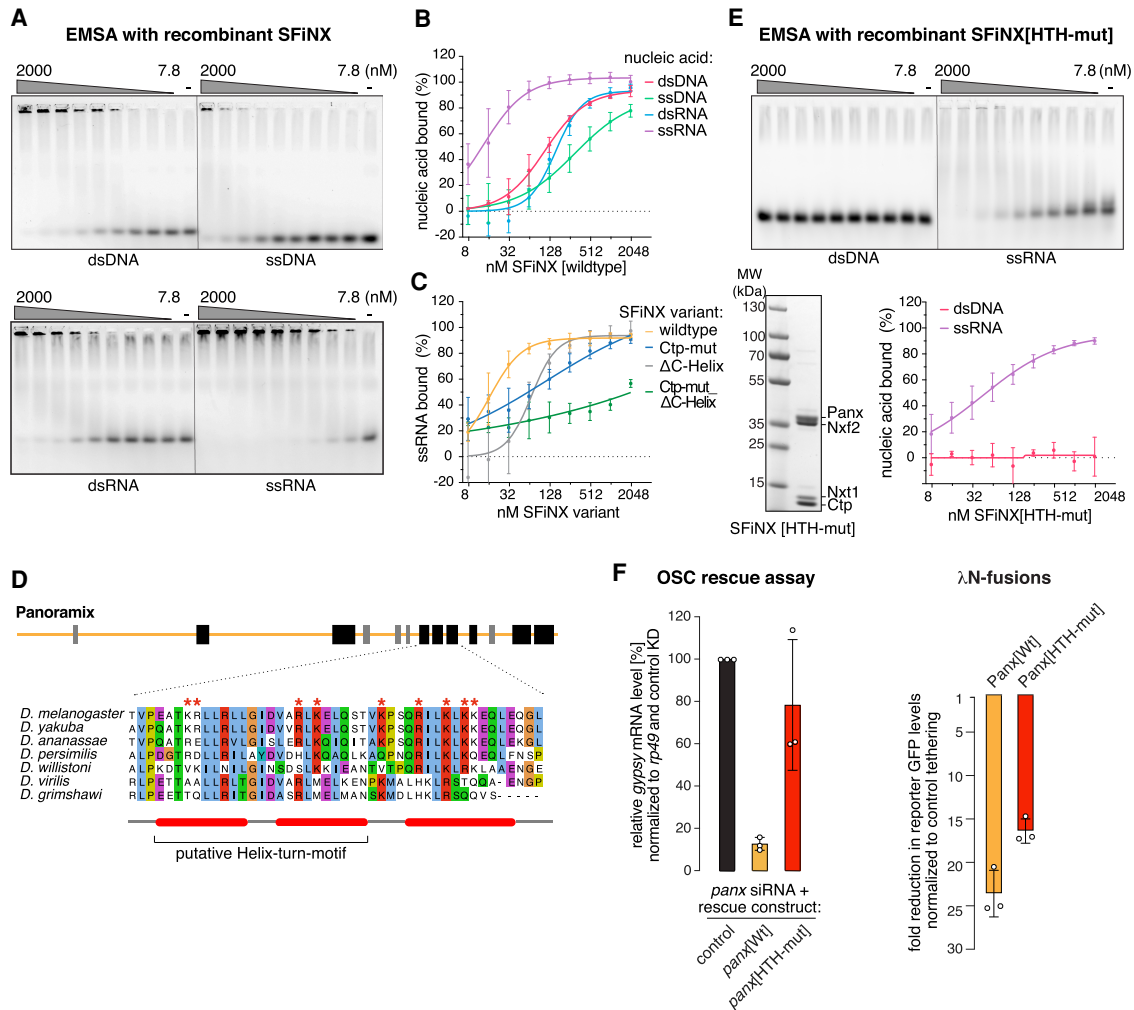


**Figure 6.** SFiNX interacts with nucleic acids. (A) Agarose gel images showing electrophoresis mobility shift assays (EMSA) using indicated nucleic acids (Alexa 647-labeled). Serial dilution of recombinant SFiNX[wild type] ranging from 7.8 to 2000 nM is shown (“–” indicates no protein; nucleic acid concentration: 5n+M). (B) Binding curves based on EMSA experiments in A (calculated from quantified free nucleic acid;  $n = 3$ ; error bars: SD) are shown. (C) Binding curves between ssRNA and indicated SFiNX variants are shown ( $n = 3$ ; error bars: SD). (D) Schematic representation of Panx, indicating secondary structure elements ([black]  $\alpha$  helices, [gray]  $\beta$  strands) and the putative HTH-motif below. Residues mutated in E and F are labeled with asterisks. (E, top) Agarose gel images showing electrophoresis mobility shift assays using indicated nucleic acids (Alexa 647-labeled). Serial dilution of SFiNX[wild type] ranging from 7.8 to 2000 nM is shown (“–” indicates no protein; nucleic acid concentration: 5 nM). (Bottom left) Coomassie-stained SDS PAGE showing recombinant SFiNX complex with HTH mutations. Binding curves based on EMSA experiments with SFiNX[HTH-mut] with ssRNA and dsDNA (calculated from quantified free nucleic acid;  $n = 3$ ; error bars: SD) are shown. (F, left) Bar graph showing the transposon repression rescue potential of indicated Panx expression constructs transfected into OSCs depleted of endogenous Panx. *gypsy* levels were determined via qRT-PCR ( $n = 3$  biological replicates are shown; error bars: SD). (Right) Bar diagrams showing silencing potential (GFP repression) of indicated  $\lambda$ N-fusion proteins normalized to control (data represent mean + SD of three independent experiments).

observation that recombinant SFiNX–nucleic acid complexes hardly entered the gel in our EMSA experiments (Fig. 6), we set out to investigate whether SFiNX is able to form molecular condensates in vitro, an established assay to study the ability of proteins to form multivalent interactions.

When lowering the salt concentration of a 10  $\mu$ M SFiNX solution to 150 mM NaCl or KCl, the previously clear solution rapidly became turbid due to the formation of phase-separated droplets (Fig. 7A). To characterize this process, we purified GFP-tagged SFiNX and mixed it with un-

tagged SFiNX at a ratio of one to 10. Imaging the phase separation behavior using microscopy revealed that SFiNX forms molecular condensates in a concentration-dependent manner with a threshold concentration of  $\sim 7 \mu$ M (Fig. 7A,B). The condensates were round and occasionally fused into larger round condensates, suggesting that they have liquid characteristics (Fig. 7C; Alberti et al. 2019). Using fluorescence recovery after photobleaching (FRAP), we observed a fast and complete recovery of fluorescence (Fig. 7D), confirming that SFiNX forms liquid condensates in vitro.

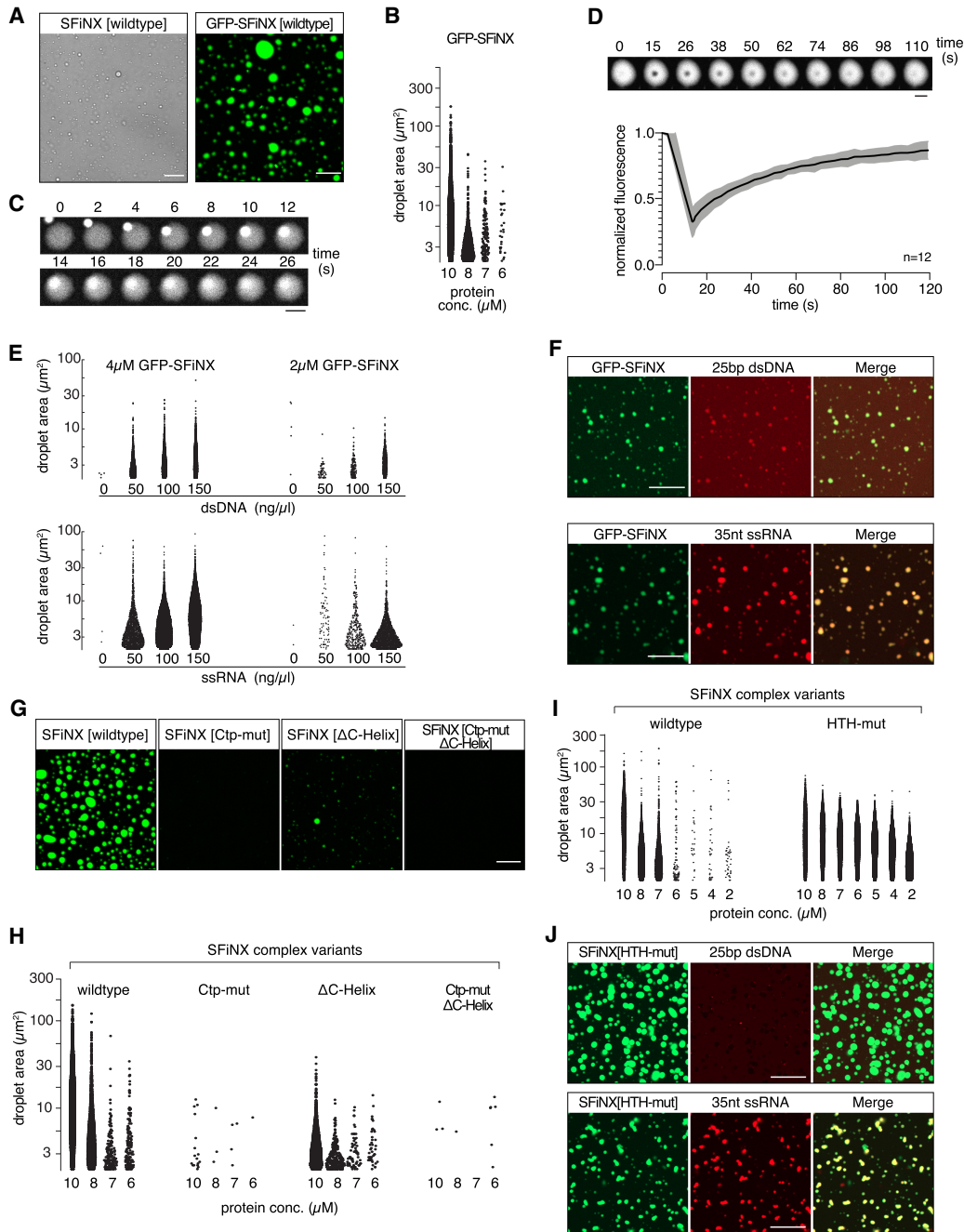


**Figure 7.** SFiNX forms molecular condensates. (A, left) Bright-field image showing SFiNX[Wt] condensates at 10  $\mu$ M. Scale bar, 20  $\mu$ m. (Right) Confocal image showing condensate formation of recombinant SFiNX at 10  $\mu$ M (containing 10% mEGFP-SFiNX). Scale bar, 20  $\mu$ m. (B) Shown are droplet number and area per droplet (sum of three microscopic fields of view) of recombinant SFiNX condensates (with mEGFP-SFiNX at 1:10) at indicated protein concentration. (C) Time-lapse series showing fusion event of two SFiNX condensates (differing intensities are due to the bigger droplet being photobleached prior to the fusion event). Scale bar, 5  $\mu$ m. (D, top) Time-lapse series showing recovery after partial photobleaching of SFiNX condensates (confocal image: representative experiment). Scale bar, 5  $\mu$ m. (Bottom) Quantification of FRAP data.  $n = 12$  experiments; SD in gray. (E) Shown are droplet number and area per droplet (sum of three microscopic fields of view) of SFiNX condensates (with mEGFP-SFiNX at 1:10) at indicated protein dsDNA (top) and ssRNA (bottom) concentrations. (F) Confocal images (scale bar, 20  $\mu$ m) showing enrichment of Alexa 647-labeled double-stranded DNA (top) or single-stranded RNA (bottom) in condensates of mEGFP-SFiNX (4  $\mu$ M). (G) Confocal images showing ability of indicated, fluorescein-labeled SFiNX variants (concentration: 10  $\mu$ M; scale bar, 20  $\mu$ m) to form condensates. (H) Shown are droplet number and area per droplet of three microscopic fields of fluorescein-labeled SFiNX variants at indicated concentration (from representative images in G; Supplemental Fig. S7C). (I) Shown are droplet number and area per droplet of three microscopic fields of fluorescein-labeled SFiNX variants at indicated concentration (from representative images in Supplemental Fig. S7D). (J) Confocal images (scale bar, 20  $\mu$ m) showing enrichment (ssRNA) or exclusion (dsDNA) of Alexa 647-labeled nucleic acids in condensates of fluorescein-labeled SFiNX[HTH-mut] (4  $\mu$ M).

Considering SFiNX's ability to bind to nucleic acids (Fig. 6), we investigated whether the presence of ssRNA or dsDNA impacts its liquid–liquid phase separation behavior. Both ssRNA as well as dsDNA substantially stimulated the formation of SFiNX condensates (Fig. 7E; Supplemental Fig. S7A,B), lowering the saturation concentration of SFiNX to 2  $\mu$ M. Consistent with this and with the previous EMSA experiments, labeled ssRNA or dsDNA copartitioned into SFiNX condensates (Fig. 7F). In conclusion, the recombinant SFiNX complex used in our experiments, despite it lacking discernible intrinsically disordered or low-complexity regions, can form molecular condensates in a nucleic acid-stimulated manner.

If multivalent interactions intrinsic to SFiNX are important for its cotranscriptional silencing activity, monomeric SFiNX, which is incapable of cotranscriptional silencing (Fig. 5), should be defective in condensate formation. We studied the phase separation properties of recombinant SFiNX variants lacking either the C-terminal helices, the dimerization protein Ctp, or both (Fig. 7G, H; Supplemental Fig. S7C). In order to visualize and quantify droplet formation, we added 5% of fluorescein-labeled complexes to unlabeled complexes. Phase separation behavior of wild-type SFiNX was comparable with that of the GFP-tagged complex. In contrast, SFiNX complexes with weakened dimerization ability showed a moderate (Pax[ $\Delta$ C-helix]) to severe (Pax[Ctp-mut]) reduction in condensate formation. Monomeric SFiNX (Pax[Ctp-mut\_ $\Delta$ C-helix]) was unable to form condensates. Thus, the ability of SFiNX to form multivalent interactions, just as its cotranscriptional silencing capacity, requires its dimerization. The strength of the *in vivo* phenotype observed for the different SFiNX dimerization mutants correlated precisely with their phase separation ability *in vitro* (wild-type > Pax[ $\Delta$ C-helix] > Pax[Ctp-mut] > Pax[Ctp-mut\_ $\Delta$ C-helix]). This argues that multivalent interactions contribute critically to SFiNX's cotranscriptional silencing capacity. It also predicts that the dimeric, yet DNA-binding-defective SFiNX complex, which is capable of cotranscriptional silencing in the tethering assay (Fig. 6E,F), should still be capable of condensate formation. Indeed, the SFiNX variant containing Pax[HTH mutant] formed molecular condensates with a saturation concentration five times lower than that of the wild-type complex (Fig. 7I; Supplemental Fig. S7D). Consistent with the EMSA results, dsDNA was excluded from the condensates (Fig. 7J), supporting the incapability of this SFiNX variant to interact with DNA. Taken together, our data point to the critical importance of multivalent interactions within the SFiNX complex for empowering the unstructured, N-terminal Pax domain to establish heterochromatin in a cotranscriptional manner.

## Discussion

In this work, we investigated the molecular characteristics that enable the SFiNX complex within the *Drosophila* piRNA pathway to mediate heterochromatin formation

when targeted to nascent RNAs via Piwi. We show that SFiNX homodimerization is required for cotranscriptional silencing but that it is dispensable for SFiNX to signal to the heterochromatin machinery. Similar findings were reported by Hannon and colleagues (Eastwood et al. 2021). Studying recombinant SFiNX, we demonstrate that dimeric SFiNX forms multivalent interactions in a nucleic acid-stimulated manner, suggesting that SFiNX multivalency and potentially the formation of molecular condensates play critical roles at piRNA target loci. Using mutational studies, we show that the ability of recombinant SFiNX to form condensates *in vitro* correlates precisely with its capacity to induce heterochromatin formation in a cotranscriptional manner *in vivo*. This argues that SFiNX multivalency, enhanced by nucleic acid binding, enables corecruited silencing activities to efficiently modify the underlying chromatin locus, potentially by increasing the dwell time of the nascent target RNA at the site of transcription.

The nuclear SFiNX concentration is expected to be considerably lower than the saturation concentration of  $\sim 7 \mu$ M at which condensate formation is observed *in vitro*. Consistent with this, microscopically detectable SFiNX condensates are not seen in wild-type cells. However, transposon transcripts harbor dozens to hundreds of complementary piRNA target sites, which would recruit, via Piwi, multiple SFiNX molecules to the site of transcription, thereby elevating SFiNX concentration locally. We propose that this might nucleate the formation of molecular condensates at piRNA target sites in a process stimulated by nascent RNA and the underlying DNA locus. Such a model would explain why single piRNA target sites are insufficient to induce cotranscriptional silencing (Post et al. 2014) and why increasing the number of Piwi or SFiNX target sites in a reporter gene leads to highly synergistic silencing responses (Post et al. 2014; Yu et al. 2015).

Also in fission yeast, oligomerization of the RNA-induced transcriptional silencing (RITS) complex (Verdel et al. 2004) is critically involved in small RNA-guided heterochromatin formation. The RITS complex consists of siRNA-loaded Ago1, Tas3, and Chp1 (Verdel et al. 2004). RITS binds target RNAs via Ago1 and it recruits chromatin-modifying factors (Grewal 2010; Holloch and Moazed 2015; Martienssen and Moazed 2015). Two additional activities are required for silencing. First, Chp1 harbors a chromodomain that binds the H3K9 methyl mark (Maksimov et al. 2018). The RITS complex can therefore tether the nascent target RNA to the underlying chromatin locus once it has been modified by the H3K9 methyltransferase complex. Second, Tas3 mediates RITS complex oligomerization via its C-terminal,  $\alpha$ -helical domain (Li et al. 2009), which is required for spreading of the silencing response at the target locus. These parallels suggest that multivalent interactions and tethering of the target RNA at chromatin are general phenomena in small RNA-guided cotranscriptional silencing processes. Formation of molecular condensates and RNA retention at chromatin has also been implicated in mammalian X chromosome inactivation (Cerase et al. 2019) and in the function of long noncoding RNAs at chromatin

(Daneshtar et al. 2020). Our work now links small RNA guided cotranscriptional gene silencing to the importance of nucleic acid-stimulated multivalent interactions in gene regulatory and chromatin-related processes.

The biochemical characterization of SFiNX was only possible through the identification of the dynein light chain Ctp as a fourth SFiNX subunit. Ctp/LC8 is a highly conserved protein in animals (96.6% identity between flies and humans). Ctp enables the dimerization of a large variety of proteins and protein complexes (Barbar 2008; Rapali et al. 2011b). Our data support the view that LC8 proteins mediate the homodimerization of protein complexes rather than bridging different client proteins in heterodimeric complexes. Intrinsic dimerization activities flanking Ctp/LC8 binding sites (like the C-terminal  $\alpha$ -helices in Panx) are probably involved in promoting homodimeric assemblies, which are then stabilized through Ctp/LC8 binding. This would prevent the erroneous formation of nonfunctional heterodimers. In the case of SFiNX, dimerization is required for its *in vitro* ability to form molecular condensates and to bind nucleic acids. Besides SFiNX, we show that several other nuclear protein complexes are Ctp/LC8 clients and hence act as homodimers. While the precise molecular role of dimerization in other Ctp/LC8 client complexes may differ, it is possible that stimulating nucleic acid binding and enabling condensate formation by promoting multivalent interactions of protein complexes may be common to many nuclear molecular machines.

## Materials and methods

### Fly strains

Supplemental Table S4 lists all used fly strains, available from the VDRC (<http://stockcenter.vdrc.at/control/main>). Before analysis, flies were aged for 4 d at 25°C on apple juice agar plates with yeast paste. Rescue lines with Panx variants were generated as described (Batki et al. 2019). Point mutations in the Ctp interaction sites of the endogenous *panx* locus were generated as described (Gokcezade et al. 2014) using an HDR donor oligo and guide RNAs listed in Supplemental Table S5. Guide RNAs were cloned into the pCFD4 plasmid via PCR followed by Gibson assembly.

### OSC cell culture

OSCs were cultured as described (Niki et al. 2006; Saito et al. 2009). For plasmid and siRNA transfections, Cell Line Nucleofector kit V (Amaxa Biosystems) with the program T-029 was used (six Mio. cells per transfection; siRNA sequences) (Supplemental Table S6).

### Generation of endogenously tagged OSC cell lines

The HDR template for N-terminal tagging of Ctp and Eggless consisted of a Puromycin-resistance followed by a P2A cleavage site followed by FLAG-GFP. The tagging construct was flanked by ~500-bp homology arms around the start codon of the respective gene and was cloned into pBluescriptII SK (+). Purified HDR PCR product (2500 ng) combined with 1500 ng of guide RNA expression plasmid (Addgene 49330) containing guide RNAs (Supplemental Table S5) were transfected into OSCs. After 2 d, cells

were plated, and 24 h later puromycin-containing medium (5  $\mu$ g/mL) was added to select for clones for 4 d. After an additional 7 d of growth, individual clones were picked and expanded. Successful tagging was analyzed by PCR, FACS, and western blot. For C-terminal tagging of Panx, a GFP-FLAG tag followed by a puromycin resistance gene driven by the *traffic jam* enhancer and a *Drosophila* synthetic core promoter was used.

### Coimmunoprecipitation of endogenously tagged proteins

OSC/mES cells were collected and washed with PBS. For isolation of nuclei, cells were resuspended in buffer 1 (10 mM Tris-HCl at pH 7.5, 2 mM MgCl<sub>2</sub>, 3 mM CaCl<sub>2</sub>, Roche Complete protease inhibitor), incubated for 20 min at 4°C followed by a centrifugation step. The pellet was resuspended in buffer 2 (10 mM Tris-HCl at pH 7.5, 2 mM MgCl<sub>2</sub>, 3 mM CaCl<sub>2</sub>, 0.5% IGEPAL CA-630, 10% glycerol, Roche Complete Protease Inhibitor), incubated for 10 min at 4°C followed by centrifugation. Isolated nuclei were lysed in buffer 3 (20 mM HEPES at pH 7.5, 150 mM NaCl, 2 mM MgCl<sub>2</sub>, 0.3% Triton X-100, 0.25% IGEPAL CA-630, 10% glycerol, Roche Complete protease inhibitor), incubated for 20 min at 4°C followed by sonication using a Diagenode Bioruptor for 10 min (30 sec on/off) at low intensity. The lysate was cleared by centrifugation and incubated for 2 h at 4°C with magnetic GFP-Trap agarose (Chromotek). The beads were washed three times for 10 min with buffer 3 and were either used for mass spectrometry analysis or the proteins were eluted in 1× SDS buffer with 5-min incubation at 95°C for western analysis. For coimmunoprecipitation of Ctp from OSCs and ovaries, cells were directly lysed in buffer 3 and processed as described above.

### Western blot

Western blot was carried out as described in Batki et al. (2019). For LC8/Dynll1 immunoblotting, 15% SDS PAGE and 0.2  $\mu$ m of PVDF membrane were used. Antibodies are listed in Supplemental Table S7.

### Immunofluorescence staining of ovaries

Immunofluorescence staining was performed as described in Batki et al. (2019). The mounted samples were imaged with a Zeiss LSM-780 confocal microscope. Antibodies are listed in Supplemental Table S7.

### Tethering reporter assay

Tethering reporter assays were performed as described (Batki et al. 2019). Fold repression compared with control experiments was calculated using 2500 cells per experiment (GFP intensity measured by FACS). For tethering of Ctp and Nxf2 in combination with RNAi, siRNAs were transfected, and after 2 d, a second transfection with siRNAs and tethering plasmid was carried out. Western blots to confirm depletion of proteins and FACS to monitor GFP expression were performed on day 5.

### RT-qPCR

RT-qPCR was performed as previously described (Batki et al. 2019). Supplemental Table S5 lists qPCR primers used.

### Fertility measurements

Virgins of respective genotypes were mated with *w<sup>1118</sup>* males. After aging for 4 d, ~10 females were put in cages with apple juice

agar plates containing yeast paste and allowed to lay eggs for 15 h. Hatching rates of laid eggs were determined 24 h after removal of flies by manual scoring.

#### CUT&RUN

CUT&RUN (protocol V.3) was performed according to Meers et al. (2019) with minor modifications. In brief, 500,000 OSCs were bound to 10  $\mu$ L of Concanavalin A-coated magnetic beads (Polysciences 86057-3) and lysed using Dig wash buffer (20 mM HEPES at pH 7.3, 150 mM NaCl, 0.5 mM spermidine, 0.01% digitonin, Roche Complete protease inhibitor EDTA). Bead-bound cells were incubated with 0.5  $\mu$ g of respective antibody (Supplemental Table S7) at 4°C overnight on a nutator. Afterward, cells were washed twice, resuspended in Dig wash buffer containing 700 ng/mL pAG-MNase (produced in house), and incubated for 1 h at 4°C on a nutator. Cells were washed twice and resuspended in Dig-wash buffer containing 2 mM  $\text{Ca}^{2+}$  to activate pAG-MNase. Reaction was stopped by the addition of 2 $\times$  STOP buffer, and samples were incubated at 500 rpm for 15 min at 37°C mixing to release DNA fragments into solution. After centrifugation, 0.1% SDS and 0.2  $\mu$ g/ $\mu$ L Proteinase K were added to the supernatant and samples were incubated for 1 h at 55°C. DNA was purified using a DNA purification kit and libraries were prepared following the manufacturer's instructions with NEBNext Ultra II DNA library preparation kit for Illumina. Sequencing was performed on a HiSeqV4 using 50-bp single-end mode.

#### Data analysis

For whole-genome analysis of CUT&RUN data, sequencing reads were aligned to the fly reference genome (dm6 assembly) using Bowtie2 (Galaxy v. 2.3.4.3) with zero mismatches allowed. Only nonduplicated, uniquely mapped reads were retained for further analysis. The plots to visualize the distribution of H3K9me3 around euchromatic transposon insertion sites (Sien-ski et al. 2015) were generated using ngs.plot (v.2.61).

#### Endogenous tagging of mouse ES cells

The homology directed repair (HDR) template for N-terminal tagging of Dynl1 contained the epitope recognized by the BC2-nanobody followed by a 3xFLAG and an AID tag. Approximately 500-bp-long homology arms flanked the start codon of the Dynl1 gene. The HDR template was cloned into the TOPO backbone, and guide RNAs were cloned into the guide RNA expression plasmid (Addgene 71707) containing an mCherry expression cassette. Plasmids were cotransfected into An3-12 mES cells stably expressing Tir1 from the Rosa26 locus using Lipofectamine 2000. After 2 d, mCherry-expressing cells were FACS-sorted and sparsely plated to allow growth of individual clones. After 7 d of growth, individual clones were picked and characterized with PCR and western blot (Supplemental Table S5 lists guide RNA sequences).

#### Mass spectrometry

Mass spectrometry was carried out as described in Batki et al. (2019).

#### Enrichment analysis of Ctp/LC8 binding sites in coimmunoprecipitation experiments

Enrichment analysis for Ctp/LC8 binding motives was done by gene set enrichment analysis (GSEA) using the fold enrichment of the identified proteins in the indicated coimmunoprecipitation

experiments as the rank metric score and LC8 hub (Jespersen et al. 2019) to predict Ctp/LC8 binding motives.

#### Protein expression and purification

For crystallization, *Drosophila melanogaster* Ctp (residues 1–89), as well as Panx peptides (residues 455–466 [Panx1], 467–480 [Panx2], and 455–480 [Panx1 + 2]) were cloned into a modified R5Fduet-1 vector (Novagen) with an N-terminal His6-SUMO tag on the Panx peptides and no tag on Ctp. Panx and Ctp were coexpressed in *Escherichia coli* strain BL21(DE3) RIL (Stratagene). The cells were grown at 37°C until OD600 reached 0.8, then the media was cooled to 16°C and IPTG was added to a final concentration of 0.35 mM to induce protein expression overnight at 16°C. The cells were harvested by centrifugation at 4°C and disrupted by sonication in binding buffer (20 mM Tris-HCl at pH 8.0, 500 mM NaCl, 20 mM imidazole) supplemented with 1 mM PMSF and 3 mM  $\beta$ -mercaptoethanol. After centrifugation, the supernatant containing complexes of Panx and Ctp was loaded onto a 5-mL HisTrap Fastflow column (GE Healthcare). After extensive washing with binding buffer, the complex was eluted with binding buffer supplemented with 500 mM imidazole. The His6-SUMO tag was removed by Ulp1 protease digestion during dialysis against binding buffer and separated by reloading onto a HisTrap column. The flow-through fraction was further purified by HiTrap Q FF column and a Superdex 75 16/60 column (GE Healthcare). The pooled fractions were concentrated to 15 mg/mL in crystallization buffer (20 mM Tris-HCl at pH 7.5, 200 mM NaCl, 1 mM DTT). The Panx mutants were generated by site-directed mutagenesis with a QuickChange kit (Agilent) and confirmed by sequencing. To carry out ITC experiments, the Panx peptides and Ctp carrying a His6-SUMO tag were expressed in isolation and purified otherwise as described above.

Coexpression of protein complexes in insect cells was carried out as described (Batki et al. 2019). An N-terminal His6 tag was fused to Ctp (or to Panx in case the respective complex didn't contain Ctp). Cell pellets were resuspended in lysis buffer (50 mM Tris at pH 8.0, 300 mM NaCl, 2 mM DTT, 0.3% TritonX-100, Roche Complete Protease Inhibitor, benzonase) followed by sonication for 10 min (1 sec on, 2 sec off) at 10% intensity using a Branson 450 Digital Sonifier. The lysates were cleared by centrifugation and loaded onto a 5-mL HisTrap HP column (GE Healthcare). After washing with buffer A (50 mM Tris at pH 8.0, 300 mM NaCl, 2 mM DTT), the bound proteins were eluted through a gradient elution targeting 500 mM Imidazole in buffer A. Peak fractions were pooled and diluted to 120 mM NaCl using buffer A with 0 mM NaCl. The protein was loaded on a HiTrapQ HP anion exchange column (GE Healthcare) and eluted in a gradient from 120 to 600 mM NaCl. Fractions containing the proteins of interest were pooled and concentrated using Amicon Ultra-15 30K spin concentrators (Merck Millipore) before further purification using a HiLoad 16/600 Superdex 200 prep grade size exclusion column (GE Healthcare) in storage buffer (40 mM HEPES at pH 7.9, 300 mM NaCl, 1 mM TCEP, 5% glycerol). The pooled fractions of interest were concentrated using Amicon Ultra-15 30K spin concentrators (Merck Millipore) to  $\sim$ 8 mg/mL, aliquoted, flash-frozen, and stored at  $-80^\circ\text{C}$  until usage.

#### Crystallization, data collection, and structure determination

Crystals of Panx-Ctp complexes were grown from different solutions (Panx1 + 2-Ctp: 0.2 M  $\text{Li}_2\text{SO}_4$ , 0.1 M Tris at pH 8.5, 40% [v/v] PEG 400; Panx1-Ctp: 0.1 M  $\text{NH}_4\text{Ac}$ , 0.1 M Bis-Tris at pH 5.5, 17% [w/v] PEG 10000; Panx2-Ctp: 0.1 M KSCN, 30% [w/v] PEG 2000 MME) using the hanging drop vapor diffusion method at 20°C. For

data collection, the crystals were flash-frozen (100 K) and collected on NE-CAT beam lines 24ID-C and 24ID-E at the Advanced Photo Source (APS), Argonne National Laboratory. The diffraction data were processed with iMosflm (Battye et al. 2011) or the NECAT RAPD online server (Kabsch 2010). The structures of Panx-Ctp complexes were solved by molecular replacement in PHENIX (Adams et al. 2002) using the structure of LC8 in complex with Nek9 peptide (PDB 3ZKE) (Gallego et al. 2013). The resulting model was completed manually using COOT (Emsley et al. 2010) and PHENIX refinement (Adams et al. 2002). The statistics of the diffraction and refinement data are summarized in Supplemental Table S3. Molecular graphics were generated with PyMOL (<https://pymol.org/2>).

#### *Size exclusion chromatography with in-line multiangle light scattering (SEC-MALS)*

SEC-MALS experiments were performed by using an Äkta-MALS system. For the analysis of Ctp in complex with Panx peptides, proteins (500  $\mu$ L) at a concentration of 1 mg/mL were loaded on a Superdex 75 10/300 GL column (GE Healthcare) and eluted with HEPES buffer (20 mM HEPES at pH 7.5, 200 mM NaCl) at a flow rate of 0.2 mL/min. SFiNX complex variants were injected at 2 mg/mL (40  $\mu$ L) on a Superdex 200 increase 3.2/300 column and eluted in storage buffer without glycerol (40 mM HEPES at pH 7.9, 300 mM NaCl, 1 mM TCEP) at a flow rate of 0.07 mL/min. Light scattering was monitored on a miniDAWN TREOS system (Wyatt Technologies). Molecular masses of proteins were analyzed using the Astra program (Wyatt Technologies).

#### *Isothermal titration calorimetry*

ITC-based binding experiments were performed on a MicroCal ITC200 calorimeter at 20°C. Panx peptides and Ctp were purified in the same buffer (20 mM Tris at pH 7.5, 150 mM NaCl, 2 mM  $\beta$ -mercaptoethanol). Panx peptides at the concentration of 200  $\mu$ M (syringe) were titrated into 15  $\mu$ M Ctp protein in the cell. The exothermic heat of reaction was measured by sequential injections of 2  $\mu$ L of the peptides into protein solution with 180-sec interval spacing. The data were fitted using the program Origin with one site model.

#### *OSC rescue assay*

OSC rescue assays were carried out as previously described (Batki et al. 2019). Each independent biological replicate was normalized to the respective control per experiment.

#### *EMSA*

Alexa 647-labeled nucleic acids (5 nM; IDT) were incubated with indicated protein concentrations in a total of 20  $\mu$ L of EMSA binding buffer (20 mM HEPES at pH 7.9, 150 mM NaCl, 1 mM MgCl<sub>2</sub>, 2.5%, 0.5 mM TCEP, 1.3  $\mu$ g/ $\mu$ L BSA) and incubated for 30 min on ice to reach equilibrium (Supplemental Fig. S6A). Four microliters of EMSA loading buffer (50% glycerol, 0.075% bromophenol blue) was added to the samples before running them on a 2% (w/v) agarose gel in 0.5 $\times$  TBE + 2.25 mM MgCl<sub>2</sub> at 80 V for ~1.5 h. Gels were imaged on a ChemiDoc acquisition system (Bio-Rad). Free nucleic acids were quantified using ImageJ, and results were fit using the Hill equation using a least square regression. Oligos used for EMSA assays are listed in Supplemental Table S5.

#### *In vitro droplet formation assay*

PEGylated plates for microscopy were prepared as described (Gibson et al. 2019). Before performing droplet formation, wells were passivated using 100 mg/mL BSA for 30 min and rinsed with ddH<sub>2</sub>O. To induce condensate formation, proteins were prepared at 2 $\times$  concentration in protein storage buffer (300 mM NaCl) and then diluted to 150 mM NaCl with ddH<sub>2</sub>O. For testing the effect of nucleic acids on condensate formation, the indicated concentrations were prepared as a 2 $\times$  mix in ddH<sub>2</sub>O. Condensates were allowed to settle for 30 min in PEGylated microscopy plates before imaging. Z-stacks consisting of 11 slices and a Z-stack step size of 0.64  $\mu$ m of three different areas per condition were acquired on an Olympus spinning disk confocal microscope equipped with a 20 $\times$ /0.75 UPLSApo WD 0.6-mm objective and Hamamatsu Orca Flash 4.0 camera. The focal plane for imaging was automatically determined using an IX3 Z-Drift Compensator, and the images were acquired using the 488 laser. FRAP assays and RNA condensate colocalization were done on a Zeiss LSM-980 confocal microscope by imaging a single confocal plane.

#### *Quantification of condensates*

Quantification of condensates was done in ImageJ. First, a maximum intensity projection of Z-stack was made followed by background subtraction using a rolling ball radius of 50. Automatic thresholding was done using the Triangle algorithm, and the condensate area was quantified by analyzing particles with a minimum size of 2  $\mu$ m<sup>2</sup> and a circularity of 0.9–1. The droplet area was plotted using R.

#### *Data and code availability statement*

Coordinates and structure factors of Ctp in complex with Panx peptides were deposited in the Protein Data Bank (PDB; accessions 7K3K, 7K3L and 7K3J). Sequencing data sets were deposited in the NCBI GEO archive (accession GSE159424). The proteomics data were deposited in the ProteomeXchange Consortium via the PRIDE partner repository (data set PXD022010).

### Competing interest statement

The authors declare no competing interests.

### Acknowledgments

We thank K. Meixner for experimental support, A. Meinhart and A. Vogel for biochemical advice, S. Schweighofer for image analysis advice, and M. Siomi for Eggless antibody. We thank the Vienna BioCenter Core Facilities (Protein Technologies, Next-Generation Sequencing, Vienna *Drosophila* Resource Center) for their support. The Institute of Molecular Biotechnology of the Austrian Academy of Sciences (IMBA) Stem Cell Core Facility generated tagged mES cells and the Gregor Mendel Institute of Molecular Plant Biology (GMI)/IMBA/Research Institute of Molecular Pathology (IMP) Bio-optics unit advised on confocal analyses. We thank G. Riddihough (<http://lifescienceditors.com>) for comments on the manuscript; the Brennecke laboratory, in particular, L. Baumgartner, D. Handler, C. Yu, and K. Senti for support; D. Gerlich and L. Cochella for feedback on the manuscript; and S. Saha for discussions. The Brennecke laboratory is supported by the Austrian Academy of Sciences, the European Community (ERC-2015-CoG-682181), and the Austrian Science Fund (F4303 and W1207). X-ray diffraction studies were

conducted at the Advanced Photon Source on the Northeastern Collaborative Access Team beamlines, supported by National Institute of General Medical Sciences grant P30 GM124165 and US Department of Energy grant DE-AC02-06CH11357. The Eiger 16M detector on 24-ID-E beamline is funded by a National Institutes of Health-Office of Research Infrastructure Programs HEI grant (S10OD021527). ITC experiments were performed in the Serzanov laboratory (New York University) with help from A. Kaushik. This work was supported in part by the Maloris Foundation (to D.J.P.). The Memorial Sloan Kettering Cancer Center structural biology core facility is supported by National Cancer Institute Core grant P30-CA008748. The work of K.M. was financed by the European Proteomics Infrastructure Consortium Providing Access (EPIC-XS), Project 823839, the Horizon 2020 Program of the European Union, and the Austrian Science Fund (ERA-CAPSI3686). U.H. was supported by a Swiss National Science Foundation Early Postdoc Mobility fellowship (P2GEP3\_188343), and M.G. was supported by the Vienna International Postdoctoral Program (VIP<sup>2</sup>) Post-Doc fellowship program (part of EU Horizon 2020 research and innovation program; Marie Skłodowska-Curie grant no. 847548).

**Author contributions:** J.S. and J. Batki identified Ctp as SFiNX subunit. J.S. performed all molecular and fly experiments, except for the following: U.H. performed SFiNX SEC-MALS experiments; M.G. performed CUT&RUN experiments and analysis; V.I.A. performed Panx co-IP; and K.P. mapped Woc/Tlk Ctp interaction sites. J.W. generated, purified, and grew crystals of Ctp-Panx complexes and performed X-ray crystallographic analyses, Ctp peptide SEC-MALS, and ITC measurements under supervision of D.J.P. N.F. generated tagged mES cells, P.D. generated fly stocks, and M.N. generated phylogenetic comparisons. K.M. supervised mass spectrometry. The project was supervised by J. Brennecke, D.J.P., and C.P., and J.S. and J. Brennecke wrote the paper with input from all authors.

## References

- Adams PD, Grosse-Kunstleve RW, Hung LW, Ioerger TR, McCoy AJ, Moriarty NW, Read RJ, Sacchettini JC, Sauter NK, Terwilliger TC. 2002. PHENIX: building new software for automated crystallographic structure determination. *Acta Crystallogr D Biol Crystallogr* **58**: 1948–1954. doi:10.1107/S0907444902016657
- Alberti S, Gladfelter A, Mittag T. 2019. Considerations and challenges in studying liquid–liquid phase separation and biomolecular condensates. *Cell* **176**: 419–434. doi:10.1016/j.cell.2018.12.035
- Allshire RC, Madhani HD. 2018. Ten principles of heterochromatin formation and function. *Nat Rev Mol Cell Biol* **19**: 229–244. doi:10.1038/nrm.2017.119
- Aravin AA, Hannon GJ, Brennecke J. 2007. The Piwi-piRNA pathway provides an adaptive defense in the transposon arms race. *Science* **318**: 761–764. doi:10.1126/science.1146484
- Barbar E. 2008. Dynein light chain LC8 is a dimerization hub essential in diverse protein networks. *Biochemistry* **47**: 503–508. doi:10.1021/bi701995m
- Batki J, Schnabl J, Wang J, Handler D, Andreev VI, Stieger CE, Novatchkova M, Lampersberger L, Kauneckaitė K, Xie W, et al. 2019. The nascent RNA binding complex SFiNX licenses piRNA-guided heterochromatin formation. *Nat Struct Mol Biol* **26**: 720–731. doi:10.1038/s41594-019-0270-6
- Battye TG, Kontogiannis L, Johnson O, Powell HR, Leslie AG. 2011. iMOSFLM: a new graphical interface for diffraction-image processing with MOSFLM. *Acta Crystallogr D Biol Crystallogr* **67**: 271–281. doi:10.1107/S0907444910048675
- Brennecke J, Aravin AA, Stark A, Dus M, Kellis M, Sachidanandan R, Hannon GJ. 2007. Discrete small RNA-generating loci as master regulators of transposon activity in *Drosophila*. *Cell* **128**: 1089–1103. doi:10.1016/j.cell.2007.01.043
- Cerase A, Armaos A, Neumayer C, Avner P, Guttman M, Tartaglia GG. 2019. Phase separation drives X-chromosome inactivation: a hypothesis. *Nat Struct Mol Biol* **26**: 331–334. doi:10.1038/s41594-019-0223-0
- Cox DN, Chao A, Lin H. 2000. piwi encodes a nucleoplasmic factor whose activity modulates the number and division rate of germline stem cells. *Development* **127**: 503–514.
- Czech B, Munafò M, Ciabrelli F, Eastwood EL, Fabry MH, Kneuss E, Hannon GJ. 2018. piRNA-guided genome defense: from biogenesis to silencing. *Annu Rev Genet* **52**: 131–157. doi:10.1146/annurev-genet-120417-031441
- Daneshvar K, Ardehali MB, Klein IA, Hsieh FK, Kratkiewicz AJ, Mahpour A, Cancelliere SOL, Zhou C, Cook BM, Li W, et al. 2020. lncRNA DIGIT and BRD3 protein form phase-separated condensates to regulate endoderm differentiation. *Nat Cell Biol* **22**: 1211–1222. doi:10.1038/s41556-020-0572-2
- Dick T, Ray K, Salz HK, Chia W. 1996. Cytoplasmic dynein (ddlc1) mutations cause morphogenetic defects and apoptotic cell death in *Drosophila melanogaster*. *Mol Cell Biol* **16**: 1966–1977. doi:10.1128/MCB.16.5.1966
- Eastwood EL, Jara KA, Bornelöv S, Munafò M, Frantzis V, Kneuss E, Barbar EJ, Czech B, Hannon GJ. 2021. Dimerisation of the PICTS complex via LC8/Cut-up drives co-transcriptional transposon silencing in *Drosophila*. *Elife* **10**: e65557. doi:10.7554/eLife.65557
- Emsley P, Lohkamp B, Scott WG, Cowtan K. 2010. Features and development of Coot. *Acta Crystallogr D Biol Crystallogr* **66**: 486–501. doi:10.1107/S0907444910007493
- Erdős G, Szaniszló T, Pajkos M, Hajdu-Soltész B, Kiss B, Pál G, Nyitray L, Dosztányi Z. 2017. Novel linear motif filtering protocol reveals the role of the LC8 dynein light chain in the Hippo pathway. *PLoS Comput Biol* **13**: e1005885. doi:10.1371/journal.pcbi.1005885
- Fabry MH, Ciabrelli F, Munafò M, Eastwood EL, Kneuss E, Falciani I, Falconio FA, Hannon GJ, Czech B. 2019. piRNA-guided co-transcriptional silencing coopts nuclear export factors. *Elife* **8**: e47999. doi:10.7554/eLife.47999
- Fan J, Zhang Q, Tochio H, Li M, Zhang M. 2001. Structural basis of diverse sequence-dependent target recognition by the 8 kDa dynein light chain. *J Mol Biol* **306**: 97–108. doi:10.1006/jmbi.2000.4374
- Fedoroff NV. 2012. Transposable elements, epigenetics, and genome evolution. *Science* **338**: 758–767. doi:10.1126/science.338.6108.758
- Font-Burgada J, Rossell D, Auer H, Azorin F. 2008. *Drosophila* HP1c isoform interacts with the zinc-finger proteins WOC and Relative-of-WOC to regulate gene expression. *Genes Dev* **22**: 3007–3023. doi:10.1101/gad.481408
- Gallego P, Velazquez-Campoy A, Regué L, Roig J, Reverter D. 2013. Structural analysis of the regulation of the DYNLL/LC8 binding to Nek9 by phosphorylation. *J Biol Chem* **288**: 12283–12294. doi:10.1074/jbc.M113.459149
- Ghildiyal M, Zamore PD. 2009. Small silencing RNAs: an expanding universe. *Nat Rev Genet* **10**: 94–108. doi:10.1038/nrg2504
- Gibson BA, Doolittle LK, Schneider MWG, Jensen LE, Gamarra N, Henry L, Gerlich DW, Redding S, Rosen MK. 2019. Organization of chromatin by intrinsic and regulated phase separation. *Cell* **179**: 470–484.e21. doi:10.1016/j.cell.2019.08.037

- Gokcezade J, Sienski G, Duchek P. 2014. Efficient CRISPR/Cas9 plasmids for rapid and versatile genome editing in *Drosophila*. *Genetics* **196**: 2279–2282. doi:10.1534/genetics.114.014126
- Goldman CH, Neiswender H, Veeranan-Karmegam R, Gonsalvez GB. 2019. The Egalitarian binding partners Dynein light chain and Bicardal-D act sequentially to link mRNA to the Dynein motor. *Development* **146**: dev176529. doi:10.1242/dev.176529
- Grewal SI. 2010. RNAi-dependent formation of heterochromatin and its diverse functions. *Curr Opin Genet Dev* **20**: 134–141. doi:10.1016/j.gde.2010.02.003
- Holoch D, Moazed D. 2015. RNA-mediated epigenetic regulation of gene expression. *Nat Rev Genet* **16**: 71–84. doi:10.1038/nrg3863
- Iwasaki YW, Murano K, Ishizu H, Shibuya A, Iyoda Y, Siomi MC, Siomi H, Saito K. 2016. Piwi modulates chromatin accessibility by regulating multiple factors including histone H1 to repress transposons. *Mol Cell* **63**: 408–419. doi:10.1016/j.molcel.2016.06.008
- Janssen A, Colmenares SU, Karpen GH. 2018. Heterochromatin: guardian of the genome. *Annu Rev Cell Dev Biol* **34**: 265–288. doi:10.1146/annurev-cellbio-100617-062653
- Jespersen N, Estelle A, Waugh N, Davey NE, Blikstad C, Ammon YC, Akhmanova A, Ivarsson Y, Hendrix DA, Barbar E. 2019. Systematic identification of recognition motifs for the hub protein LC8. *Life Sci Alliance* **2**: e201900366. doi:10.26508/lsa.201900366
- Kabsch W. 2010. Integration, scaling, space-group assignment and post-refinement. *Acta Crystallogr D Biol Crystallogr* **66**: 133–144. doi:10.1107/S0907444909047374
- Kessler R, Tisserand J, Font-Burgada J, Reina O, Coch L, Attolini CS, Garcia-Bassets I, Azorín F. 2015. Ddsk2 regulates H2Bub1 and RNA polymerase II pausing at dHP1c complex target genes. *Nat Commun* **6**: 7049. doi:10.1038/ncomms8049
- Kidane AI, Song Y, Nyarko A, Hall J, Hare M, Löhr F, Barbar E. 2013. Structural features of LC8-induced self-association of swallow. *Biochemistry* **52**: 6011–6020. doi:10.1021/bi400642u
- Koch CM, Honemann-Capito M, Egger-Adam D, Wodarz A. 2009. Windei, the *Drosophila* homolog of mAM/MCAF1, is an essential cofactor of the H3K9 methyl transferase dSETDB1/Eggless in germ line development. *PLoS Genet* **5**: e1000644. doi:10.1371/journal.pgen.1000644
- Le Thomas A, Rogers AK, Webster A, Marinov GK, Liao SE, Perkins EM, Hur JK, Aravin AA, Toth KF. 2013. Piwi induces piRNA-guided transcriptional silencing and establishment of a repressive chromatin state. *Genes Dev* **27**: 390–399. doi:10.1101/gad.209841.112
- Li H, Motamedi MR, Yip CK, Wang Z, Walz T, Patel DJ, Moazed D. 2009. An  $\alpha$  motif at Tas3 C terminus mediates RITS cis spreading and promotes heterochromatic gene silencing. *Mol Cell* **34**: 155–167. doi:10.1016/j.molcel.2009.02.032
- Liang J, Jaffrey SR, Guo W, Snyder SH, Clardy J. 1999. Structure of the PIN/LC8 dimer with a bound peptide. *Nat Struct Biol* **6**: 735–740. doi:10.1038/11501
- Lo KW, Naisbitt S, Fan JS, Sheng M, Zhang M. 2001. The 8-kDa dynein light chain binds to its targets via a conserved (K/R) XTQT motif. *J Biol Chem* **276**: 14059–14066. doi:10.1074/jbc.M010320200
- Makokha M, Hare M, Li M, Hays T, Barbar E. 2002. Interactions of cytoplasmic dynein light chains Tctex-1 and LC8 with the intermediate chain IC74. *Biochemistry* **41**: 4302–4311. doi:10.1021/bi011970h
- Maksimov V, Oya E, Tanaka M, Kawaguchi T, Hachisuka A, Ekwall K, Bjering P, Nakayama JI. 2018. The binding of Chp2's chromodomain to methylated H3K9 is essential for Chp2's role in heterochromatin assembly in fission yeast. *PLoS One* **13**: e0201101. doi:10.1371/journal.pone.0201101
- Martienssen R, Moazed D. 2015. RNAi and heterochromatin assembly. *Cold Spring Harb Perspect Biol* **7**: a019323. doi:10.1101/cshperspect.a019323
- Meers MP, Bryson TD, Henikoff JG, Henikoff S. 2019. Improved CUT&RUN chromatin profiling tools. *Elife* **8**: e46314. doi:10.7554/eLife.46314
- Mugat B, Nicot S, Varela-Chavez C, Jourdan C, Sato K, Basyuk E, Juge F, Siomi MC, Pélisson A, Chambeyron S. 2020. The Mi-2 nucleosome remodeler and the Rpd3 histone deacetylase are involved in piRNA-guided heterochromatin formation. *Nat Commun* **11**: 2818. doi:10.1038/s41467-020-16635-5
- Murano K, Iwasaki YW, Ishizu H, Mashiko A, Shibuya A, Kondo S, Adachi S, Suzuki S, Saito K, Natsume T, et al. 2019. Nuclear RNA export factor variant initiates piRNA-guided co-transcriptional silencing. *EMBO J* **38**: e102870. doi:10.15252/emboj.2019102870
- Mutlu B, Chen HM, Moresco JJ, Orelo BD, Yang B, Gaspar JM, Keppler-Ross S, Yates JR, Hall DH, Maine EM, et al. 2018. Regulated nuclear accumulation of a histone methyltransferase times the onset of heterochromatin formation in *C. elegans* embryos. *Sci Adv* **4**: eaat6224. doi:10.1126/sciadv.aat6224
- Narlikar GJ. 2020. Phase-separation in chromatin organization. *J Biosci* **45**: 5.
- Niki Y, Yamaguchi T, Mahowald AP. 2006. Establishment of stable cell lines of *Drosophila* germ-line stem cells. *Proc Natl Acad Sci* **103**: 16325–16330. doi:10.1073/pnas.0607435103
- Ninova M, Chen YA, Godneeva B, Rogers AK, Luo Y, Fejes Tóth K, Aravin AA. 2020. Su(var)2-10 and the SUMO pathway link piRNA-guided target recognition to chromatin silencing. *Mol Cell* **77**: 556–570.e6. doi:10.1016/j.molcel.2019.11.012
- O'Shea EK, Klemm JD, Kim PS, Alber T. 1991. X-ray structure of the GCN4 leucine zipper, a two-stranded, parallel coiled coil. *Science* **254**: 539–544. doi:10.1126/science.1948029
- Osumi K, Sato K, Murano K, Siomi H, Siomi MC. 2019. Essential roles of Windei and nuclear monoubiquitination of Eggless/SETDB1 in transposon silencing. *EMBO Rep* **20**: e48296. doi:10.15252/embr.201948296
- Ozata DM, Gainetdinov I, Zoch A, O'Carroll D, Zamore PD. 2018. PIWI-interacting RNAs: small RNAs with big functions. *Nat Rev Genet* **20**: 89–108. doi:10.1038/s41576-018-0073-3
- Pfister KK, Shah PR, Hummerich H, Russ A, Cotton J, Annar AA, King SM, Fisher EM. 2006. Genetic analysis of the cytoplasmic dynein subunit families. *PLoS Genet* **2**: e1. doi:10.1371/journal.pgen.0020001
- Phillis R, Statton D, Caruccio P, Murphey RK. 1996. Mutations in the 8 kDa dynein light chain gene disrupt sensory axon projections in the *Drosophila* imaginal CNS. *Development* **122**: 2955–2963.
- Post C, Clark JP, Sytnikova YA, Chirn GW, Lau NC. 2014. The capacity of target silencing by *Drosophila* PIWI and piRNAs. *RNA* **20**: 1977–1986. doi:10.1261/rna.046300.114
- Rapali P, Radnai L, Süveges D, Harmat V, Tölgyesi F, Wahlgren WY, Katona G, Nyitray L, Pál G. 2011a. Directed evolution reveals the binding motif preference of the LC8/DYNLL hub protein and predicts large numbers of novel binders in the human proteome. *PLoS One* **6**: e18818. doi:10.1371/journal.pone.0018818
- Rapali P, Szenes A, Radnai L, Bakos A, Pál G, Nyitray L. 2011b. DYNLL/LC8: a light chain subunit of the dynein motor complex and beyond. *FEBS J* **278**: 2980–2996. doi:10.1111/j.1742-4658.2011.08254.x

- Rozhkov NV, Hammell M, Hannon GJ. 2013. Multiple roles for Piwi in silencing *Drosophila* transposons. *Genes Dev* **27**: 400–412. doi:10.1101/gad.209767.112
- Saito K, Nishida KM, Mori T, Kawamura Y, Miyoshi K, Nagami T, Siomi H, Siomi MC. 2006. Specific association of Piwi with rasiRNAs derived from retrotransposon and heterochromatic regions in the *Drosophila* genome. *Genes Dev* **20**: 2214–2222. doi:10.1101/gad.1454806
- Saito K, Inagaki S, Mituyama T, Kawamura Y, Ono Y, Sakota E, Kotani H, Asai K, Siomi H, Siomi MC. 2009. A regulatory circuit for piwi by the large Maf gene *traffic jam* in *Drosophila*. *Nature* **461**: 1296–1299. doi:10.1038/nature08501
- Senti KA, Brennecke J. 2010. The piRNA pathway: a fly's perspective on the guardian of the genome. *Trends Genet* **26**: 499–509. doi:10.1016/j.tig.2010.08.007
- Shimada Y, Mohn F, Bühler M. 2016. The RNA-induced transcriptional silencing complex targets chromatin exclusively via interacting with nascent transcripts. *Genes Dev* **30**: 2571–2580. doi:10.1101/gad.292599.116
- Sienski G, Dönertas D, Brennecke J. 2012. Transcriptional silencing of transposons by Piwi and Maelstrom and its impact on chromatin state and gene expression. *Cell* **151**: 964–980. doi:10.1016/j.cell.2012.10.040
- Sienski G, Batki J, Senti KA, Dönertas D, Tirian L, Meixner K, Brennecke J. 2015. Silencio/CG9754 connects the Piwi-piRNA complex to the cellular heterochromatin machinery. *Genes Dev* **29**: 2258–2271. doi:10.1101/gad.271908.115
- Silljé HH, Nigg EA. 2001. Identification of human Asf1 chromatin assembly factors as substrates of Tousled-like kinases. *Curr Biol* **11**: 1068–1073. doi:10.1016/S0960-9822(01)00298-6
- Siomi MC, Sato K, Pezic D, Aravin AA. 2011. PIWI-interacting small RNAs: the vanguard of genome defence. *Nat Rev Mol Cell Biol* **12**: 246–258. doi:10.1038/nrm3089
- Slotkin RK, Martienssen R. 2007. Transposable elements and the epigenetic regulation of the genome. *Nat Rev Genet* **8**: 272–285. doi:10.1038/nrg2072
- Thurmond J, Goodman JL, Strelets VB, Attrill H, Gramates LS, Marygold SJ, Matthews BB, Millburn G, Antonazzo G, Trovisco V, et al. 2019. Flybase 2.0: the next generation. *Nucleic Acids Res* **47**: D759–D765. doi:10.1093/nar/gky1003
- Verdel A, Jia S, Gerber S, Sugiyama T, Gygi S, Grewal SI, Moazed D. 2004. RNAi-mediated targeting of heterochromatin by the RITS complex. *Science* **303**: 672–676. doi:10.1126/science.1093686
- Wang SH, Elgin SC. 2011. *Drosophila* Piwi functions downstream of piRNA production mediating a chromatin-based transposon silencing mechanism in female germ line. *Proc Natl Acad Sci* **108**: 21164–21169. doi:10.1073/pnas.1107892109
- Wang L, Hare M, Hays TS, Barbar E. 2004. Dynein light chain LC8 promotes assembly of the coiled-coil domain of swallow protein. *Biochemistry* **43**: 4611–4620. doi:10.1021/bi036328x
- Yang P, Wang Y, Macfarlan TS. 2017. The role of KRAB-ZFPs in transposable element repression and mammalian evolution. *Trends Genet* **33**: 871–881. doi:10.1016/j.tig.2017.08.006
- Yu Y, Gu J, Jin Y, Luo Y, Preall JB, Ma J, Czech B, Hannon GJ. 2015. Panoramix enforces piRNA-dependent cotranscriptional silencing. *Science* **350**: 339–342. doi:10.1126/science.aab0700
- Zhao K, Cheng S, Miao N, Xu P, Lu X, Zhang Y, Wang M, Ouyang X, Yuan X, Liu W, et al. 2019. A Pandas complex adapted for piRNA-guided transcriptional silencing and heterochromatin formation. *Nat Cell Biol* **21**: 1261–1272. doi:10.1038/s41556-019-0396-0